© 2020. Published by The Company of Biologists Ltd | Development (2020) 147, dev181057. doi:10.1242/dev.181057

RESEARCH ARTICLE

Lack of AKAP3 disrupts integrity of the subcellular structure and proteome of mouse sperm and causes male sterility

Kaibiao Xu[1,2,3], Lele Yang[1,2], Lan Zhang[4] and Huayu Qi[1,2,3,4,5,*]

ABSTRACT

The development and maintenance of the correct morphology of sperm is important for their functions. Cellular morphogenesis of sperm occurs during the post-meiotic developmental stage; however, little is known about what coordinates this process. In the present study, we investigated the role of A-kinase anchoring protein 3 (AKAP3) during mouse spermiogenesis, using both mouse genetics and proteomics. It was found that AKAP3 is essential for the formation of the specific subcellular structure of the sperm flagellum, motility of sperm and male fertility. Additionally, lack of AKAP3 caused global changes of the sperm proteome and mislocalization of sperm proteins, including accumulation of RNA metabolism and translation factors and displacement of PKA subunits in mature sperm, which may underlie misregulated PKA activity and immotility in sperm. Interestingly, sperm lacking a complete fibrous sheath from both *Akap3* and *Akap4* null mice accumulated F-actin filaments and morphological defects during post-testicular maturation in the epididymis. These results suggest that the subcellular structures of sperm could be formed via independent pathways, and elucidate the roles of AKAP3 during the coordinated synthesis and organization of the sperm proteome and sperm morphology.

KEY WORDS: AKAP3, PKA, Spermiogenesis, Fibrous sheath, Sperm proteome

INTRODUCTION

The male gamete, sperm, possesses highly organized cellular structures that are uniquely designed for its biological functions. The cellular morphogenesis of sperm occurs during spermiogenesis, the post-meiotic developmental stage of haploid spermatids. In mouse, spermiogenesis takes about 14 days and can be divided into four phases and 16 steps that occur through 12 cycling epithelial stages in testis according to the morphological changes of spermatids (Leblond and Clermont, 1952; Oakberg, 1956). During this period of time, spermatids synthesize proteins, transport and localize them into correct positions and rearrange or construct all necessary organelles, including highly condensed nuclei with little transcription activity, acrosome vesicles containing hydrolyzing enzymes and a well-organized flagellated tail that enables sperm to travel long distances (Gold et al., 2018; Hermo et al., 2010; Sassone-Corsi, 2002; Wachten et al., 2017). Previous studies using targeted gene deletion in mouse have uncovered functions of numerous genes that are important for the morphogenesis of sperm and fertility (Krausz and Riera-Escamilla, 2018; Matzuk and Lamb, 2008); however, how spermatids manifest this drastic cellular morphogenesis remains largely unclear.

At the ultrastructural level, each organelle of sperm is fine-tuned with various subcellular structures. For example, the flagellum of sperm tail is composed of microtubule-based cytoskeletal structures. At the center of the flagellum lies the axoneme, composed of nine microtubule doublets surrounding a central pair (the '9+2' structure). The central axoneme is surrounded by nine outer dense fibers (ODFs) running along the entire flagellum. Outside of the ODFs, a spiral mitochondrial sheath forms in the mid-piece next to the head region, followed by an electron-dense fibrous sheath (FS) in the principal piece of sperm tail. The FS can be further divided into diagonally positioned longitudinal columns (LCs) and connecting circumferential ribs (CRs) that lie in-between them. These accessary structures contain numerous proteins, including glycolytic enzymes (Eddy et al., 2003), that are essential for the regulation of sperm motility, which is powered by dynein motors attached to the axoneme using energy generated by mitochondria and the cytoplasmic glycolytic reaction (Lehti and Sironen, 2017; Nakada et al., 2006; Odet et al., 2011; Owa et al., 2019). Despite decades of research, it is still not clear whether different subcellular structures of sperm are constructed in a coordinated process or through independent pathways.

Early studies from Clermont and colleagues suggested that the flagellum is constructed in an orderly fashion. In rat sperm, the axoneme is completed early, at around step 2, when round spermatids still transcribe genes, providing a platform for the synthesis and assembly of other subcellular structures. The LCs of the FS are synthesized and assembled early at the same time but continue to mature until step 15, whereas the CRs are not assembled until step 9 around precursor substances, the anlagen, that are deposited along the axoneme earlier, following a distal-to-proximal direction. Other subcellular structures, such as the ODFs and mitochondria sheath, also form during this period of time but at different rates (Clermont et al., 1990; Irons and Clermont, 1982; Oko and Clermont, 1989). Once sperm are fully developed, they traverse through the epididymis for additional post-testicular maturation until they eventually become motile and competent for fertilizing eggs (Breton et al., 2019). Although not fully characterized, genetic mutations of genes that affect sperm morphology often cause defects in more than one subcellular structure, suggesting that cellular morphogenesis of sperm is more likely a systemically regulated process.

During spermiogenesis, round spermatids enter the elongating stage, which is accompanied by upregulation of protein synthesis

[1]CAS Key Laboratory of Regenerative Biology, South China Institute for Stem Cell Biology and Regenerative Medicine, Guangzhou Institutes of Biomedicine and Health, Chinese Academy of Sciences, Guangzhou 510630, China. [2]Guangdong Provincial Key Laboratory of Stem Cell and Regenerative Medicine, South China Institute for Stem Cell Biology and Regenerative Medicine, Guangzhou Institutes of Biomedicine and Health, Chinese Academy of Sciences, Guangzhou 510630, China. [3]University of Chinese Academy of Sciences, Beijing 100049, China. [4]GIBH-GMU Joint-school of Biological Sciences, Guangzhou Medical University, Guangzhou 511436, China. [5]Guangzhou Regenerative Medicine and Health Guangdong Laboratory, Guangzhou 510005, China.

*Author for correspondence (qi_huayu@gibh.ac.cn)

H.Q., 0000-0003-1539-5650

Received 31 May 2019; Accepted 20 November 2019

Development (2020) 147, dev181057. doi:10.1242/dev.181057

activities (Braun et al., 1989; Kleene, 2013). Hundreds of proteins are synthesized and orchestrated in order to construct the correct morphology of sperm (Iguchi et al., 2006). How developing spermatids coordinate protein synthesis with the formation of various subcellular structures and what signals are involved in the regulation of these processes are not clear. Immunocytochemical analyses suggested that protein components are synthesized and continuously added onto the anlagen within the developing flagellum until the excess cytoplasmic contents are shed in the form of residual bodies (Clermont et al., 1990; Irons and Clermont, 1982). Some early studies also showed that developing spermatids and even maturing sperm contain active translation machinery (Bragg and Handel, 1979; Ostermeier et al., 2002), suggesting that protein synthesis may occur within the developing sperm flagellum. In the same vein, irregular expression and localization of sperm proteins have been shown to underlie the etiology of male infertility diseases, including oligo-astheno-teratozoospermia (Coutton et al., 2015; Lehti and Sironen, 2017; Saraswat et al., 2017). Nonetheless, the signaling pathways and molecular underpinnings for the spatiotemporal regulation of protein synthesis in developing spermatids remain largely unexplored.

We previously found that increased PKA activity positively regulates protein synthesis in elongating spermatids at the translational level and that the PKA regulatory subunit RIα and catalytic subunit Cα are associated with translationally active poly-ribosomal fractions in testis lysates on a sucrose gradient (Xu et al., 2014). PKA signaling plays multifaceted roles during spermatogenesis and in regulating sperm functions (Burton and McKnight, 2007). Mice that are haploinsufficient for PKA RIα, reminiscent of Carney complex syndrome (CNC), appear to be male sterile due to defective sperm morphology (Burton et al., 2006). PKA activity is often refined by attachment of its regulatory subunits to AKAPs (A-kinase anchoring proteins), which restrict PKA to specific subcellular domains close to its substrates (Scott et al., 2013; Torres-Quesada et al., 2017). Several AKAP proteins have been found in sperm, of which sperm-specific AKAP3 and AKAP4 are prominent components of the FS (Carrera et al., 1994; Fulcher et al., 1995; Lin et al., 1995; Rawe et al., 2004; Vijayaraghavan et al., 1999), and probably possess different roles in sperm (Johnson et al., 1997; Mandal et al., 1999). Mice lacking the X chromosome-linked *Akap4* gene are male sterile due to their malformed FS and immotility of flagella, and *AKAP4* has been linked to human dysplasia of the fibrous sheath (DFS) (Baccetti et al., 2005; Miki et al., 2002). As a dual-specific AKAP that interacts with both RIα and RIIα, the functions of AKAP3 remain to be determined (Xu and Qi, 2014). In the present study, we analyzed the potential roles of AKAP3 during spermiogenesis and sperm motility regulation using a gene knockout mouse model. The results indicate that AKAP3 is important not only for the formation of specific subcellular structures of sperm but also for maintaining the integrity of sperm proteome, morphology and function.

RESULTS

Generation of *Akap3* gene null mice

In order to find out the functions of AKAP3 during spermiogenesis, *Akap3* gene null mice were generated using the CRISPR/Cas9 method. Two sgRNAs targeting the fifth exon of the *Akap3* genomic region were selected to introduce a mutation near the start codon. *In vitro*-transcribed mRNA of the Cas9 endonuclease and sgRNAs were microinjected into cytoplasm of two-cell embryos, which were then transplanted into foster females. Several *Akap3* null mutants obtained with various deletions showed similar phenotypes in mature sperm during initial assessments (Fig. S1A-C). One female carrying a 103-bp fragment deletion was chosen to establish the *Akap3* null mouse line for further experimentation (Fig. 1A,B). This mutation caused a frame-shift after nucleotide 223 of *Akap3* mRNA. Testis and sperm from homozygous mice did not express AKAP3 protein as shown by both western blotting and immunofluorescence staining using a specific antibody generated against the N-terminal domain of AKAP3 (Fig. 1C,D) (Xu and Qi, 2014). Using PCR of genomic DNA and direct DNA sequencing, no mutations were found at the top putative off-target sites (Table S1).

Deletion of *Akap3* causes sperm morphology abnormalities and male sterility

To examine the effect of *Akap3* mutation, mutant mice were crossed with wild-type mice. It was found that only the $Akap3^{-/-}$ male mice were unable to produce any litters over a 3-month breeding period, compared with control mating pairs, including $Akap3^{+/-}$ male and $Akap3^{-/-}$ female mice (Fig. 2A). It has been shown that AKAP4 (another AKAP protein in the FS) is important for sperm flagella formation and male fertility (Miki et al., 2002). To determine whether AKAP3 plays different roles to AKAP4, we also generated *Akap4* gene null mice (Fig. S1D-G, Table S1). Consistent with previous findings, $Akap4^{-/Y}$ male mice were sterile (Fig. 2A).

To find out whether the *Akap3* mutation caused any defects in sperm leading to male sterility, sperm isolated from the vas deferens of adult mice were examined. Compared with wild-type sperm, *Akap3* null sperm barely showed any motility in either PBS or human tubule fluid (HTF), a condition that induces capacitation, including hyperactivity, in sperm (Movies 1-6). Under a light microscope, we observed that the length of the sperm tail varies in mutant mice. Wild-type sperm have an average length of 118.41±3.23 µm (n=130), whereas both *Akap3* and *Akap4* null sperm developed tails with reduced length (100.74±19.77 µm, n=575, and 65.49±16.91 µm, n=163, respectively; P<0.001). This change in tail length is mainly due to shortening of the principal piece, as the mid-piece of the sperm appeared similar (Fig. 2B). The length of the sperm tail was measurable only for those with extended postures. However, many sperm exhibited a disorganized tail morphology, including bent/coiled or split flagella that rarely occur in wild-type sperm (Fig. 2D-F). The frequency of these abnormalities was counted within a population of sperm. About 29% and 11% of *Akap3* null sperm from vas deferens contained bent/coiled and split tails, respectively, and *Akap4* null sperm contained 41% and 6% bent/coiled and split tails, respectively (Fig. 2C). Because sperm tail is composed of microtubule cytoskeletal structures, immunostaining of α-tubulin was performed in order to view the cytoskeletal networks of sperm. Consistently, tubulin cytoskeletons in mutant sperm were found to be disorganized, with many bent/coiled or split filaments in tails (Fig. 2G-I). Sperm from $Akap4^{-/Y}$ mice seemed to be more drastically affected, consistent with previous findings (Miki et al., 2002). In addition, it was also noticed that some *Akap3* null sperm (~8%) had a mis-shaped head and retained TNP1, suggesting dysregulated nuclear condensation (Fig. S2A-C). These results suggest that both AKAP3 and AKAP4 are important for the formation of sperm flagella; however, AKAP3 may participate in the morphogenesis of sperm differently to AKAP4.

Absence of subcellular structures in *Akap3* null sperm

AKAP3 is synthesized in elongating spermatids and located specifically in the FS of the principal piece of sperm flagellum (Xu et al., 2014). To find out whether particular subcellular structures in sperm are affected by the absence of AKAP3, sperm

Development (2020) 147, dev181057. doi:10.1242/dev.181057

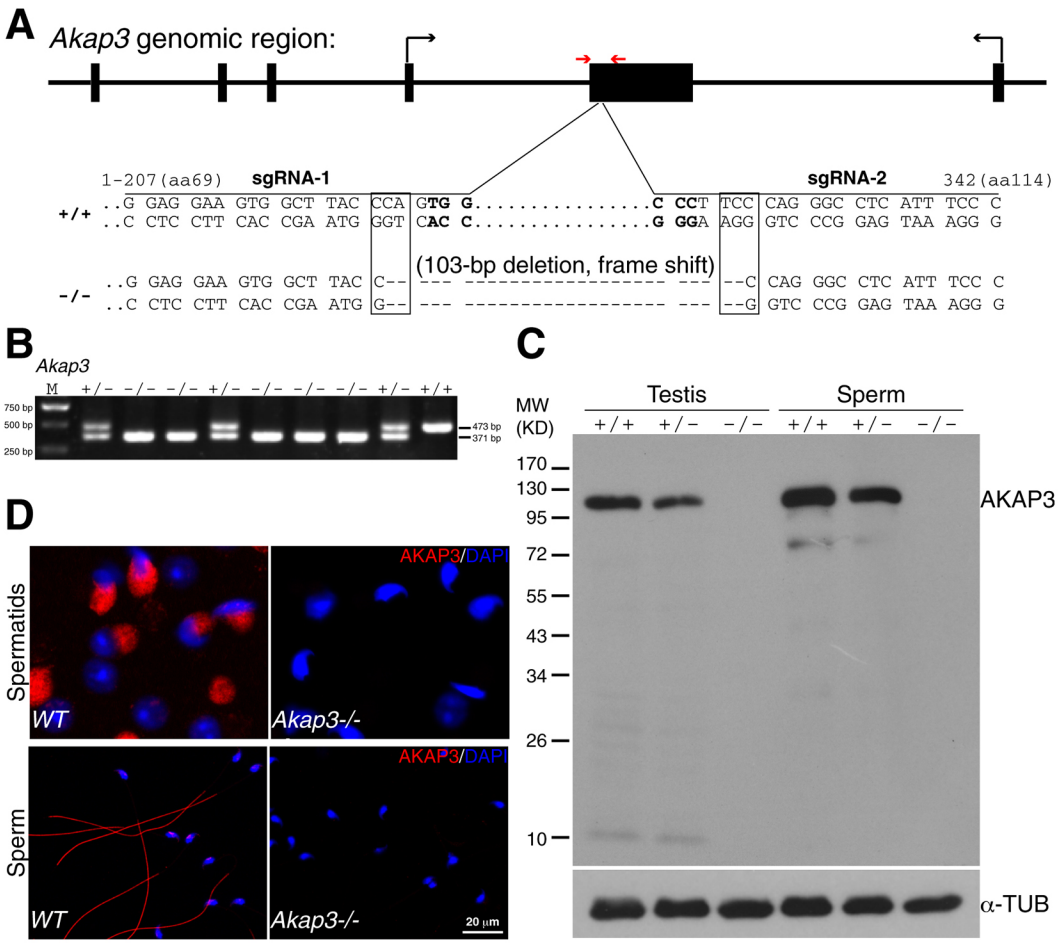

Fig. 1. Generation of *Akap3* gene null mice. (A) Schematic of the genomic region encoding AKAP3. Arrows indicate the start and stop codons of the *Akap3* transcript, respectively. Sequences of two sgRNAs used in CRISPR/Cas9 method are shown below. NGG sequences are in bold. The numbers indicate nucleotide positions of *Akap3* mRNA and corresponding amino acids. The 103-bp deletion mutation that causes a frame-shift after nucleotide 223 eliminates the production of AKAP3. Primers used for genotyping mice by PCR are indicated by red arrows. (B) Genotyping of *Akap3* null mice. (C) Western blotting of testis and sperm lysates from wild-type and *Akap3* mutant mice. α-Tubulin (α-TUB) was used as loading control. (D) Immunofluorescence staining of spermatids and sperm from wild-type (WT) and *Akap3*$^{-/-}$ mice. Sperm nuclei were stained with DAPI. Shown are merged confocal images. Scale bar: 20 µm.

isolated from vas deferens were examined using transmission electron microscopy. Compared with wild-type sperm, the junction between the mid-piece and the principal piece, namely the annulus, appeared grossly normal at the ultrastructural level, although detachment from the mid-piece was also observed (Fig. 3A). The mid-piece of mutant sperm contained seemingly organized mitochondria flanking the ODFs and axoneme (Fig. 3B). On the longitudinal sections of the principal piece, *Akap3* null sperm exhibited an electron-dense FS outside of the ODFs and axoneme, comparable to that of wild-type sperm (Fig. 3C, upper middle panel). However, a cross-section of the principal piece showed that the electron-dense material of the FS only appeared at the diagonal positions where the LCs reside, and lacked the circle of CRs of the FS (Fig. 3C, lower middle panel). Disrupted axonemes were also observed in some cross-sections (Fig. S2D). Consistent with previous findings, the entire FS structure was missing in *Akap4* null sperm (Fig. 3C, right panels). These results indicate that AKAP3 is important for the formation of specific subcellular structures, primarily the CRs of the FS, whereas AKAP4 affects the formation of the entire FS.

Early studies suggested that the subcellular structures of sperm flagella are formed in a sequential order (Clermont et al., 1990; Irons and Clermont, 1982). However, how the protein components of each compartment are synthesized and assembled is not clear. In order to determine whether the defective FS of sperm flagellum is generated due to under-development during spermiogenesis or the loss of the structure following the maturation of sperm, we examined fully developed sperm from seminiferous tubules of testis. Similar to the sperm from vas deferens, sperm from the testis of *Akap3*$^{-/-}$ mice also contained a partially formed FS lacking the CRs before entering epididymis, whereas those from *Akap4*$^{-/Y}$ mice lost the FS entirely (Fig. 3D), suggesting that the defects in subcellular structures in the sperm tail are caused by developmental deficits in the absence of AKAP proteins.

Misregulated PKA signaling during capacitation of *Akap3* null sperm

PKA activity has been shown to be important for the capacitation of sperm (Visconti et al., 1997). The structural defects in *AKAP3* or *AKAP4* null sperm could cause displacement of PKA subunits and misregulated PKA activity, leading to immotility of sperm. To test this, proteins extracted from testis and sperm were examined using western blotting. It was found that in *Akap3* null sperm, both PKA RIα and Cα were decreased, especially in SDS-extracted fractions,

Development (2020) 147, dev181057. doi:10.1242/dev.181057

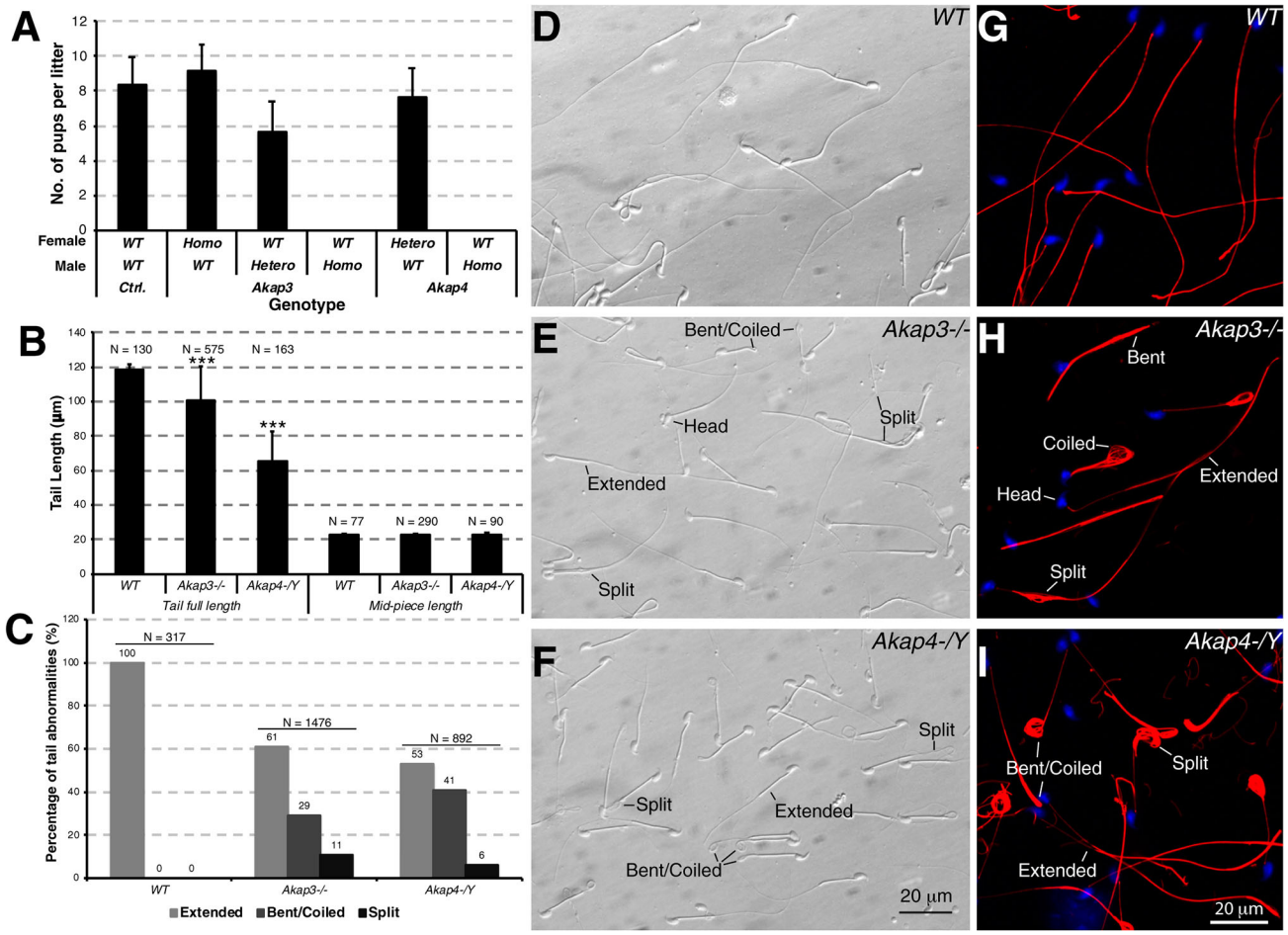

Fig. 2. Male infertility and sperm tail morphological defects caused by *Akap3* and *Akap4* gene mutations. (A) Results of fertility testing showing that homozygous mutant mice are infertile (n=8). (B) Tail length measurement of sperm. Both *Akap3* and *Akap4* null sperm have a shortened full tail length, whereas the average lengths of their mid-piece were similar to that of wild type (WT). ***P<0.001, Student's t-test. N indicates the number of sperm measured. (C) Abnormalities of sperm tails in *Akap3*$^{-/-}$ and *Akap4*$^{-/Y}$ mice. N indicates the number of tails counted within a sperm population. (D-F) Transmission light microscopy of sperm. Compared with the wild type (D), sperm from both *Akap3*$^{-/-}$ (E) and *Akap4*$^{-/Y}$ (F) mice showed extensive abnormalities in their tails. Various forms of defects are indicated. (G-I) Immunofluorescence staining of sperm. Wild-type sperm contained organized microtubules (G), whereas *Akap3* (H) and *Akap4* (I) null sperm showed disorganized microtubule bundles in their tails. Red, α-tubulin; blue, nuclei. Shown are merged confocal images. Scale bars: 20 µm.

whereas PKA RIIα remained at a similar level to that of wild-type sperm (Fig. 4A). By contrast, RIα was slightly increased in the Triton X-100-soluble fraction in *Akap4* null sperm compared with the wild-type counterpart, but no apparent changes were seen for either RIIα or Cα in *Akap4* null sperm (Fig. 4B). Consistent with this, measurement of PKA activity in sperm lysates showed that there was a modest but significant decrease in PKA activity in *Akap3* null sperm when they were capacitated in HTF (Fig. 4C). No significant changes of PKA activity were seen in *Akap4* null sperm under similar conditions. During capacitation, PKA-mediated increases of serine/threonine phosphorylation lead to subsequent protein tyrosine phosphorylation. Both phospho-serine/threonine of PKA substrates and protein tyrosine-phosphorylation are hallmarks of sperm hyperactivity (Baker et al., 2009). In agreement with PKA subunit changes in mutant sperm, western blotting of sperm lysates showed that levels of phospho-serine/threonine of PKA substrates (Fig. 4D), as well as tyrosine-phosphorylated insoluble proteins (Fig. 4E) were decreased under both basal (PBS) and capacitation (HTF) conditions, compared with their wild-type counterparts. In addition, relative quantification of immunofluorescence signals showed that phospho-serine/threonine PKA substrates were decreased mostly in the principal piece, whereas phospho-tyrosine levels were decreased in both the mid-piece and principal piece of mutant sperm tails (Fig. 4F, Fig. S3A-C). In *Akap4* null sperm, tyrosine-phosphorylated AKAP3 also appeared to be reduced (Fig. S3D). The suggestion of misregulated PKA activity is further supported by the mislocalization of PKA subunits in mutant sperm. When examined with stimulated emission depletion microscopy (STED) following immunostaining, PKA Cα appeared to decrease at the periphery of the sperm tail in the absence of AKAP3, whereas both PKA Cα and AKAP3 were more dramatically mislocated in *Akap4* null sperm, presumably due to the loss of different subcellular structures in FS (Fig. 4G, Fig. S3E). In both cases, RIIα appeared to associate with the central axoneme and showed little change in its subcellular localization. Collectively, these results indicate that the absence of AKAP3 and AKAP4 causes misregulated expression of PKA subunits and PKA activity, leading to decreased protein phosphorylation and disrupted motility in sperm.

Lack of AKAP3 caused global changes of sperm proteome

The subcellular structures of sperm are composed of various proteins that participate in different biological processes, such as signal transduction, energy generation and proteolysis-mediating functions of sperm. The lack of different subcellular structures in

Development (2020) 147, dev181057. doi:10.1242/dev.181057

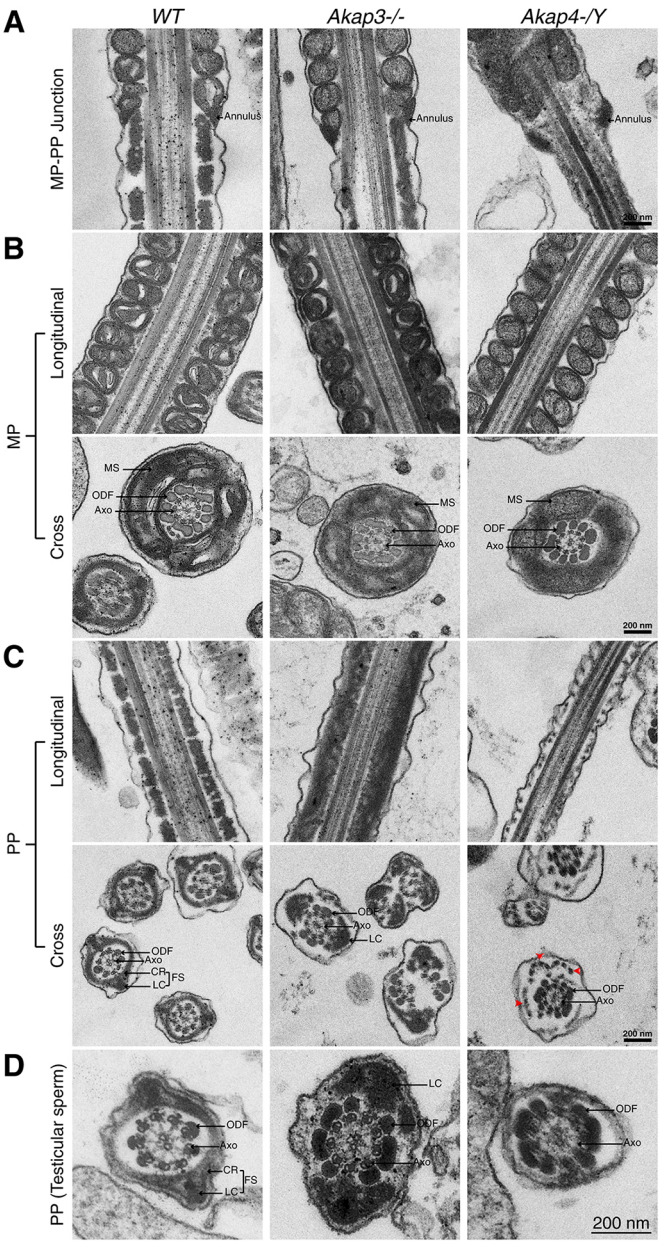

Fig. 3. Disrupted FS formation in the absence of either AKAP3 or AKAP4. (A) Transmission electron microscopic (TEM) images of the junctional region between the mid-piece (MM) and the principal piece (PP) of the sperm tail. Positions of the annulus are indicated. (B) TEM images of the mid-piece of the sperm tail. Both longitudinal and sagittal (Cross) views are shown. Axo, axoneme; MS, mitochondria sheath. (C) TEM images of the principal piece of the sperm tail. Both longitudinal and sagittal views are shown. In *Akap3* null sperm, the FS lacks circular CRs in-between two diagonally positioned LCs. Disrupted axonemes also occur in some cross-sections. *Akap4* null sperm appeared to contain no FS, with only some electron-dense material left adjacent to the plasma membrane (red arrowheads). (D) TEM images of cross-sections of the principal piece of sperm tails from seminiferous tubules. Similar to sperm from the vas deferens, the *Akap3* null sperm lacked CRs, whereas the *Akap4* null sperm were lacking the entire FS. Scale bars: 200 nm. WT, wild type.

Akap3 and *Akap4* null sperm suggested that these AKAP proteins participate in different morphogenetic processes and may affect different protein compositions in sperm. In order to find out the molecular basis of their various defects, quantitative tandem mass tagging (TMT) and protein spectrometry were applied to whole-sperm proteome. Sperm from vas deferens of adult wild-type, *Akap3*$^{-/-}$ and *Akap4*$^{-/Y}$ mice were collected and extracted under denaturing conditions. Following trypsin digestion and liquid chromatographic fractionation, proteomes of the sperm were identified by mass spectrometry (LC-MS/MS). We conducted three experimental repeats using different groups of mice at either the same time or different times. In order to obtain a general view of sperm proteome changes, the average results from the experimental repeats performed at the same time with three mice from each genotype were selected as representatives for subsequent analyses. Of these, a total of 3873 proteins were identified, similar to the total number of sperm proteins identified previously (Castaneda et al., 2017; Chauvin et al., 2012). Among them, 3349 proteins were quantitatively compared according to their peptide abundance (Fig. 5A). Compared with wild-type sperm, *Akap3* gene mutation caused a decrease of 91 and an increase of 228 proteins, whereas *Akap4* null sperm contained 45 upregulated and 45 downregulated proteins ($\geq$1.3-fold, $P<0.05$) (Fig. 5B, Tables S3 and S4). Selected proteins, including components of PKA signaling, AKAP proteins and some of the known components of sperm flagellum, showed a similar trend of changes across experimental repeats, indicating relatively consistent protein quantification (Fig. 5C). Differentially expressed sperm proteins in *Akap3* null sperm were first used for gene ontology (GO) analysis. It was found that the overall GO terms for downregulated proteins were mainly related to flagellum structure and motility regulation, including motor proteins and ion channels, indicating that cytoskeletal components and motility regulators in flagella are highly relevant for the missing subcellular structure (CRs) of the FS (Fig. 5D, upper left panel). Interestingly, proteins involved in cytosolic processes, including protein synthesis regulation, RNA and protein metabolism and actin filament regulation were enriched in sperm in the absence of AKAP3 (Fig. 5D, upper right panel). Analysis of the molecular functions of the changed proteins agreed well with this in that regulators of ion channels and PKA activity are significantly represented in the downregulated proteins, whereas poly(A) RNA-binding, ribosome/translation machinery and actin filament-associated proteins are upregulated (Fig. 5D, lower panels). This is further supported by the analysis of over-represented Reactome pathways (Fig. 5E). Interestingly, proteins expressed at differential levels in *Akap3* null sperm, compared with wild-type sperm, were not only related to the FS and cytoskeletal structures but also appeared to be associated with various cellular organelles, including the nucleus, acrosome, mitochondria, endoplasmic reticulum/Golgi and secretory vesicles, as well as cytosol and plasma membrane, indicating an unexpected global effect on the sperm proteome due to the lack of AKAP3 (Fig. 5F, upper panel). This is also the case for *Akap4* null sperm in that differentially expressed proteins are distributed across the entire cell among various subcellular structures (Fig. 5F, lower panel).

Absence of AKAP3 affects the integrity of sperm structure, causing mislocalizations of sperm proteins

Using bioinformatics, differentially expressed proteins that are associated with significantly enriched networks of functional protein hubs were identified. These analyses intend to uncover not only proteins that are known for their biological relevance but also proteins with potential links but for which functional roles remain unclear. Among the downregulated proteins, functional groups associated with potential functions of AKAP3 were identified, including cAMP-dependent protein kinase activity (AKAP3 itself and PKA subunits), regulation of dynein-related

Development (2020) 147, dev181057. doi:10.1242/dev.181057

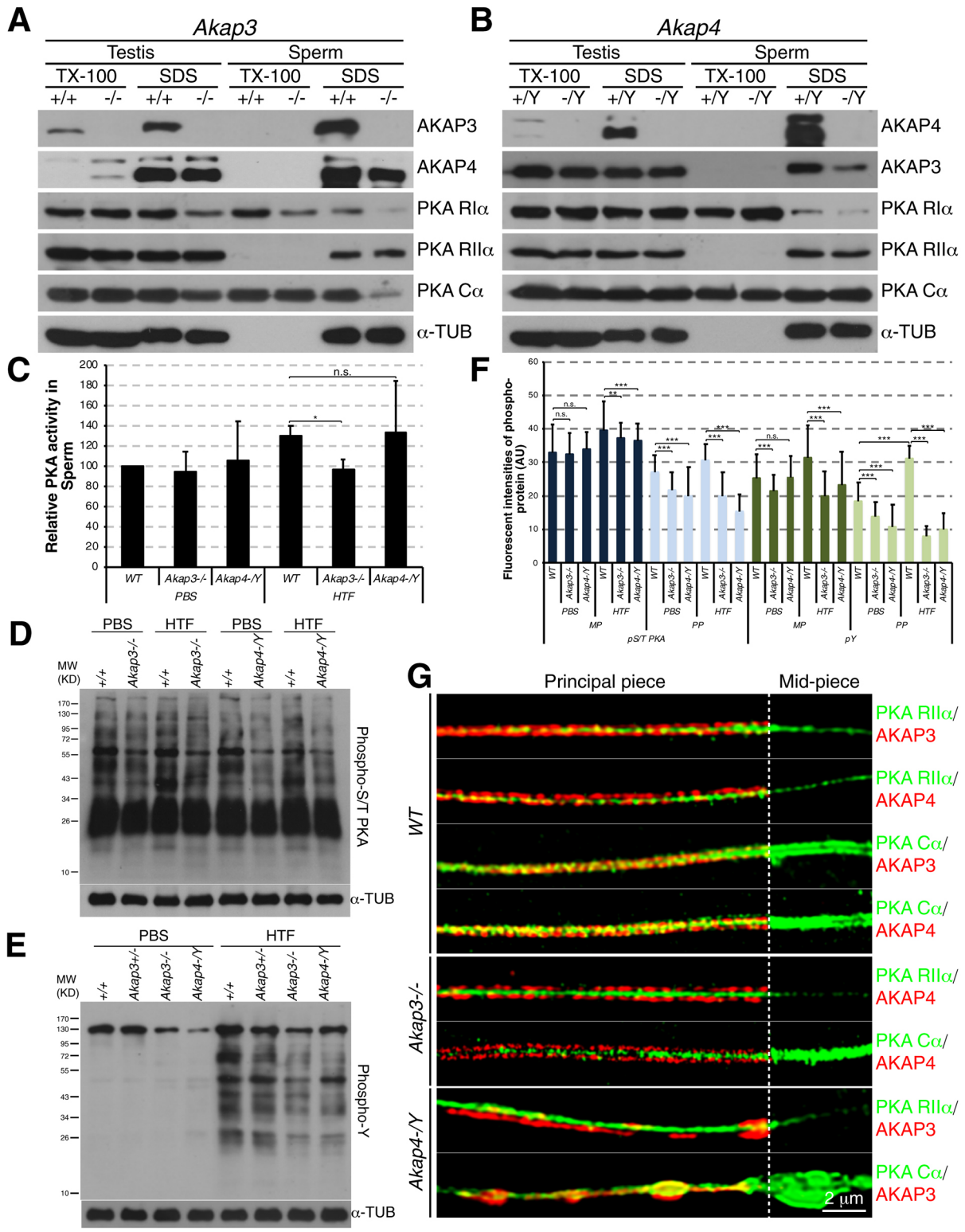

Fig. 4. See next page for legend.

motor activity and ion channel activity containing CATSPERs (cation channel in sperm) (Fig. 6A). Another downregulated group is the monosaccharide-binding proteins, including SLC2A5 and SLC2A3, for which functions during spermatogenesis or sperm motility are currently unclear. Over 200 proteins were found to be enriched in *Akap3* null sperm compared with their wild-type counterparts. The majority of these proteins can be classified into a few main networks, including metabolism and biogenesis of RNAs or proteins and regulation of actin filaments (Fig. 6B). The enrichment of RNA metabolism and protein translation regulators in the sperm proteome when the subcellular structure of the FS is compromised suggests that regulation of protein synthesis may

Development (2020) 147, dev181057. doi:10.1242/dev.181057

Fig. 4. Impaired PKA activity in *Akap3* and *Akap4* null sperm. (A,B) Western blotting of testes and sperm lysates. Lysates were prepared under non-denaturing and denaturing conditions sequentially with Triton X-100 and SDS, respectively. PKA RIα and Cα were decreased in *Akap3* null sperm (A), whereas PKA RIα was slightly increased in the Triton X-100 (TX-100) fraction of *Akap4* null sperm (B). α-Tubulin (α-TUB) was used as loading control. (C) PKA activity assay of sperm lysate. Total lysates were prepared after sperm were incubated in either PBS (basal) or HTF (capacitation). A decrease in PKA activity in *Akap3* null sperm compared with the wild type was seen when sperm were induced for capacitation. **P*<0.05 (Student's *t*-test, *n*=4). (D,E) Western blotting of phospho-proteins. Both *Akap3* and *Akap4* null sperm appeared to contain reduced levels of phospho-serine/threonine of PKA substrates in total lysates under either basal or capacitation conditions (D). Decreased levels of phospho-tyrosine in SDS fractions of sperm lysates were more apparent in mutant sperm under capacitation conditions (E). (F) Quantification of phospho-proteins in sperm tail. Comparison of fluorescent signals following immunostaining indicated that phospho-serine/threonine was decreased mostly in the principal piece of mutant sperm tails, whereas phospho-tyrosine was decreased in both the mid-piece and principal piece when stimulated for capacitation. AU, arbitrary unit of average pixels in each area of interest in confocal fluorescent images. ***P*<0.01, ****P*<0.001 (Student's *t*-test, *n*>150 for each case). n.s., not significant. (G) STED of PKA subunits in sperm. Sperm from mice with different genotypes were immunostained with antibodies against PKA RIIα or Cα (green), together with either anti-AKAP3 or anti-AKAP4 (red). White dashed line indicates the position of the mid-piece and principal piece junction. Scale bar: 2 µm. WT, wild type.

occur in the cytoplasmic domains of sperm flagellum during spermiogenesis.

To verify the proteomics analyses and gain insights into the regulation of sperm development and function, changes in several highly differentiated proteins in *Akap3* and *Akap4* null sperm were investigated using biochemical methods. Western blotting of testis and sperm lysates showed that although no significant changes at the protein level could be detected in testis lysates, the FS proteins ropporin 1 (ROPN1), ropporin 1-like (ROPN1L) and sperm autoantigenic protein 17 (SPA17) were decreased in both *Akap3* and *Akap4* null sperm. On the other hand, spermatid-associated protein (SPERT; also known as CBY2), ribosome binding protein 1 (RRBP1), cortactin (CTTN) and IQ motif containing GTPase activating protein 2 (IQGAP2) were increased in *Akap3*, but not *Akap4* null sperm, consistent with the mass spectrometry data (Fig. 6C, left panels). Dynein axonemal intermediate chain 2 (DNAI2; DNAIC2) was reduced in insoluble fractions of sperm, whereas β-actin appeared to increase in *Akap3* null, but not in *Akap4* null, sperm (Fig. 6C, right panels). Consistent with previous findings, glyceraldehyde-3-phosphate dehydrogenase testis-specific (GAPDHS) was only decreased in *Akap4* null sperm (Fig. 6C, right panels) (Miki et al., 2002).

To confirm the differentially expressed proteins within sperm, immunofluorescence staining was performed using available antibodies against candidate proteins. In agreement with the mass spectrometry and western blotting results, both SPA17 and enolase 1 (ENO1) appeared to decrease in *Akap3* and *Akap4* null sperm, whereas GAPDHS was decreased only in *Akap4* null sperm (Fig. S4A). Milk fat globule-EGF factor 8 (MFGE8), protein disulfide isomerase-like testis expressed (PDILT), RRBP1 and CTTN, on the other hand, showed increased fluorescent signals in mutant sperm tail (Fig. S4B). Interestingly, besides changes in expression levels, the subcellular localizations of some of the proteins were also altered (Fig. 6D). SPA17 was no longer seen in the FS in *Akap3* mutant sperm, suggesting that it is likely localized in the CRs of the FS. The glycolytic enzyme ENO-1 could still be seen in *Akap3* null sperm along the longitudinal direction, probably due to the remaining LCs, but was scattered along the entire sperm tail in *Akap4* null sperm when the FS could not be formed. It has been suggested that sperm contain both enolase 1 and sperm-specific enolase 4, for which functions relating to spermiogenesis and sperm motility remain to be determined (Gitlits et al., 2000; Nakamura et al., 2013). An *in vitro* glutathione S-transferase (GST) pull-down assay suggested that AKAP3 may bind enolase 1 rather than enolase 4, whereas AKAP4 can interact with both (Fig. S5). The mislocalization in sperm was also seen for MFGE8, which was no longer restricted to the post-nuclear cytoplasm and the mid-piece as in wild-type sperm and instead localized to the principal piece as well. This could be caused by impairment of sperm cytoplasm segmentation. In this regard, SEPTIN4, a member of the septin family that forms the septin ring at the annulus, was found to be mislocalized in *Akap3* and *Akap4* null sperm (Fig. S6), indicating a compromised subcellular organization in mutant sperm. Collectively, these results suggest that deletion of AKAP3 and AKAP4 not only affected the expression of the sperm proteome but also interrupted the correct subcellular localizations of proteins. These defects in the integrity of sperm at both structural and biochemical levels may underlie the causes of sperm immotility and male infertility in mutant mice.

Increased morphological abnormalities and F-actin filaments in *Akap3* and *Akap4* null sperm during post-testicular maturation in epididymis

The morphogenesis of spermatids takes place within the seminiferous tubules of the testis during post-meiotic development. In order to find out when the morphological defects occur in *Akap3*$^{-/-}$ mice, testes and spermatogenic cells were examined using immunocytochemistry. No abnormality in spermatogenic cells was detected within the testis at the cellular level, although testicular sperm already had a disrupted FS when examined at the ultrastructural level (Fig. 3D). Testes and epididymis from both *Akap3*$^{-/-}$ and *Akap4*$^{-/Y}$ mice were comparable to those of wild-type mice in appearance (Fig. S7A). On cross-sections of testes and epididymis from adult mice, spermatogenic cells at all stages could be observed (Fig. S7B). Flow cytometry of enzyme-digested adult testicular cells also displayed similar profiles showing the expected proportions of spermatogenic cells at various developmental stages, indicating that the numbers of spermatogenic cells were not changed (Fig. S8A). No differences in overall morphology between mutant and wild-type spermatids were observed when cells were stained with α-tubulin antibody (Fig. S8B,C). In addition, little difference in the expression or subcellular localizations of PKA subunits was seen in isolated round and elongating spermatids (Fig. S9).

The above results indicate that the morphological alterations in developing spermatids may be hard to observe when they are isolated or when defects in flagella only become apparent at later stages, for example after the developed sperm exit the testis and before entering the vas deferens. For this reason, sperm from epididymis and vas deferens were examined. Interestingly, it was found that the tail lengths of mutant sperm in the caput epididymis were similar to that of wild type (115.14±5.92 µm, *n*=150, and 114.63±6.10 µm, *n*=124, for *Akap3* and *Akap4* null sperm, respectively). The tail length of *Akap3* null sperm, however, gradually decreased as sperm passed through the corpus and cauda epididymis, whereas *Akap4* null sperm shortened their tail length more dramatically in the corpus epididymis (Fig. 7A, Fig. S10). The various types of sperm abnormalities, including bent/coiled and split flagella, were also gradually increased in *Akap3* null sperm as they progressed through the epididymis (Fig. 7B), whereas *Akap4* null sperm showed more abrupt changes during their traversing of the epididymis (Fig. 7C). These results suggest that the structural integrity of sperm

Development (2020) 147, dev181057. doi:10.1242/dev.181057

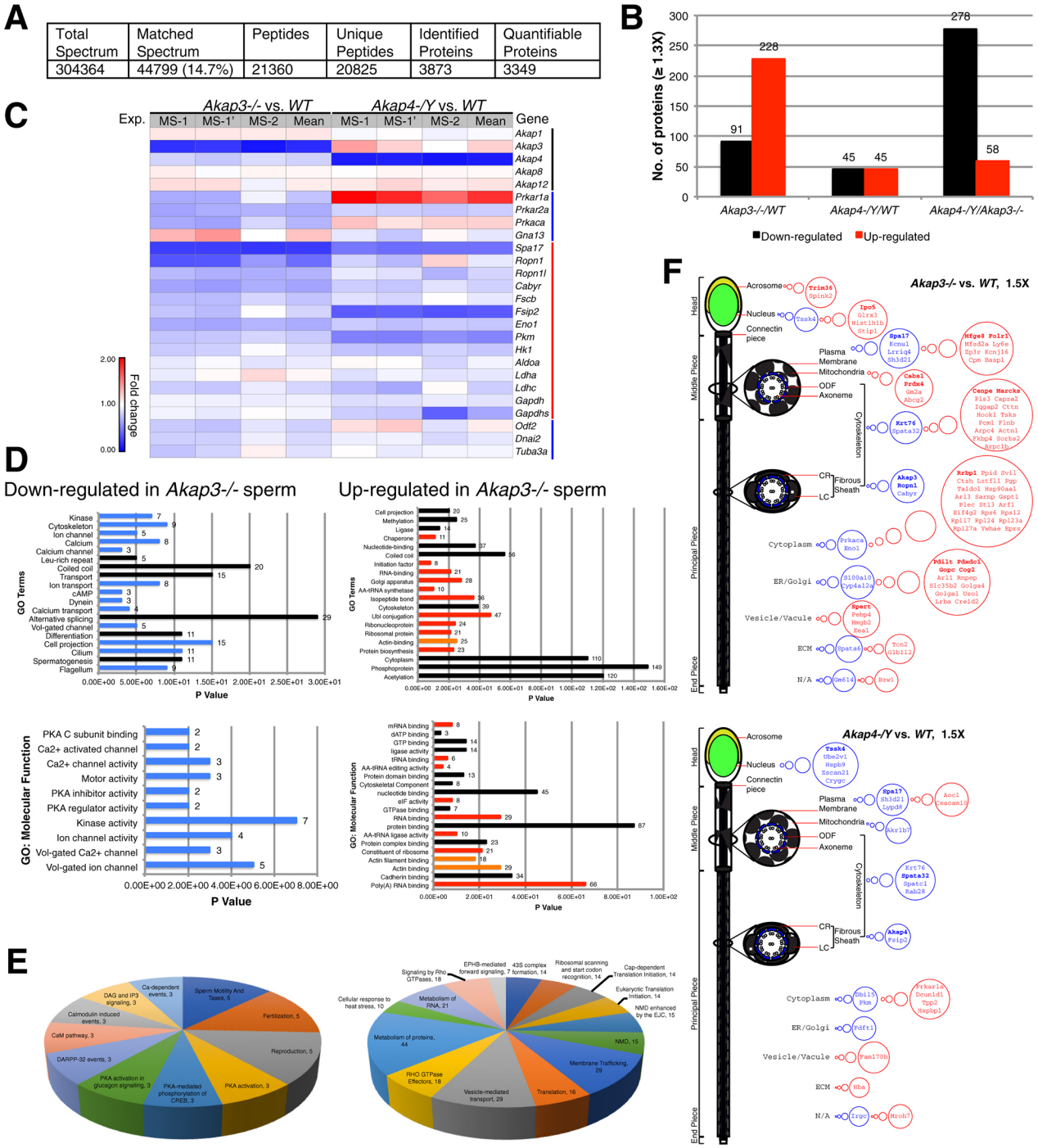

Fig. 5. *Akap3* and *Akap4* mutations caused global changes of sperm proteomes. (A) Total peptides and proteins of sperm regardless of genotypes identified in LC/MS-MS. (B) Bar graph of differentially expressed proteins commonly identified in *Akap3* and *Akap4* null sperm. Fold change: ≥1.3, P<0.05. (C) Heat map of differentially expressed sperm proteins. Fold changes of selected proteins among experimental repeats done at the same time (MS-1 and MS-1′) and at different times (MS-1 and MS-2) were compared across samples. A similar trend of changes was seen across experiments. (D) GO analysis of differentially expressed sperm proteins in *Akap3* null sperm. Distinct GO terms were found in proteins that are either decreased (blue) or increased (red and orange) in the absence of AKAP3, compared with wild-type sperm. (E) Reactome pathway analysis. Consistent with the GO analysis, decreased proteins in *Akap3* null sperm are mainly associated with PKA signaling, ion-dependent events and motility regulation, whereas the increased proteins are relevant to RNA and protein metabolism, protein translation machinery and actin cytoskeleton regulation. (F) Schematic of the cellular distributions of differentially expressed proteins in *Akap3* and *Akap4* null sperm. They were not only associated with cytoskeletal networks but were also widely distributed in different organelles, including nucleus, acrosome, endoplasmic reticulum/Golgi and plasma membrane. Blue indicates downregulation, red indicates upregulation. The size of the circles indicates the number of proteins found in this category. Proteins changed more than 2-fold are in bold. WT, wild type.

was compromised during post-testicular maturation when subcellular compartments (the CRs and LCs of FS) were missing due to the absence of either AKAP3 or AKAP4.

Mass spectrometry data indicated that regulators of actin filaments, including the RHO kinase family members and ARP2/3 actin binding factors, were enriched in *Akap3* mutant sperm (Fig. 6B).

Development (2020) 147, dev181057. doi:10.1242/dev.181057

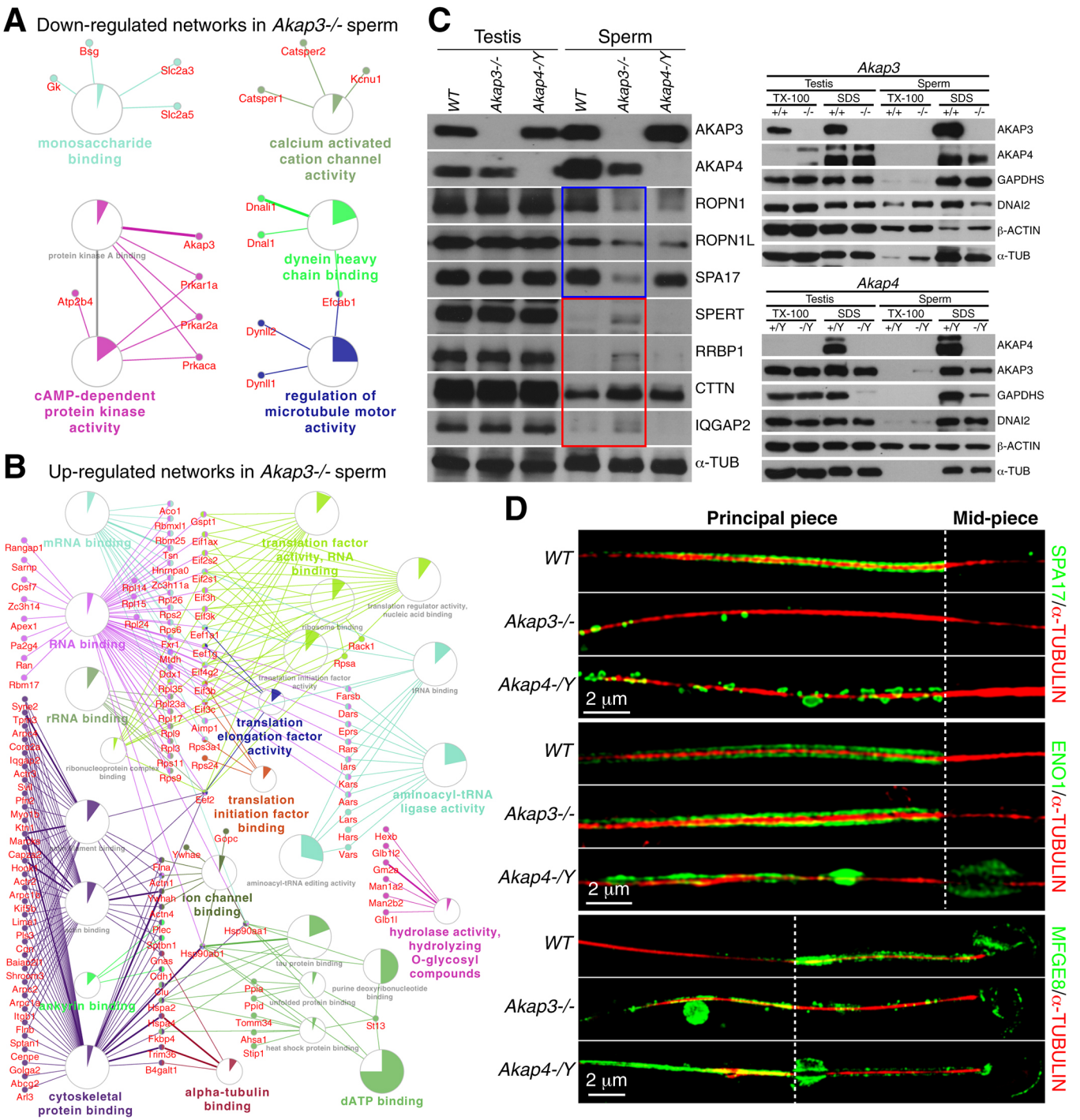

Fig. 6. Altered expression and subcellular localizations of proteins in *Akap3* and *Akap4* null sperm. (A) Protein function networks enriched in decreased proteins in *Akap3* null sperm. (B) Protein function networks involving increased proteins in *Akap3* null sperm. The node size indicates term significance; colored segment within each node indicates the percentage of mapped genes compared with all associated genes; shared colors indicate genes with overlapping functions; and line weight indicates the likelihood of genes connected to that functional group. (C) Western blotting of sperm proteins. Changes of selected decreased (blue) or increased (red) proteins in *Akap3* null sperm are consistent with the mass spectrometry data. GAPDHS was found to decrease only in *Akap4* null sperm. α-TUB, α-tubulin; TX-100, Triton X-100. (D) Subcellular localizations of sperm proteins. The localizations of differentially changed proteins were altered when there was no complete FS formed in *Akap3* or *Akap4* null sperm, suggesting the importance of an intact FS for their proper localization. White dashed lines indicate the positions of the mid-piece and principal piece junction. Shown are merged STED images. WT, wild type. Scale bars: 2 μm.

Western blotting of sperm lysates also showed an increase of β-actin in *Akap3* null sperm (Fig. 6C). The differential expression of these proteins could interfere with post-testicular maturation of sperm, as cortical actin fibers often facilitate morphological changes of cells. To examine whether actin filaments were changed in *Akap3* and *Akap4* mutants, mature sperm from wild-type, *Akap3*$^{-/-}$ and *Akap4*$^{-/Y}$ mice were immunostained with Phalloidin-FITC. During post-testicular sperm maturation, sperm acquire modifications as they traverse through epididymis (Bedford and Calvin, 1974). The fluorescent signals of F-actin appeared to increase

Development (2020) 147, dev181057. doi:10.1242/dev.181057

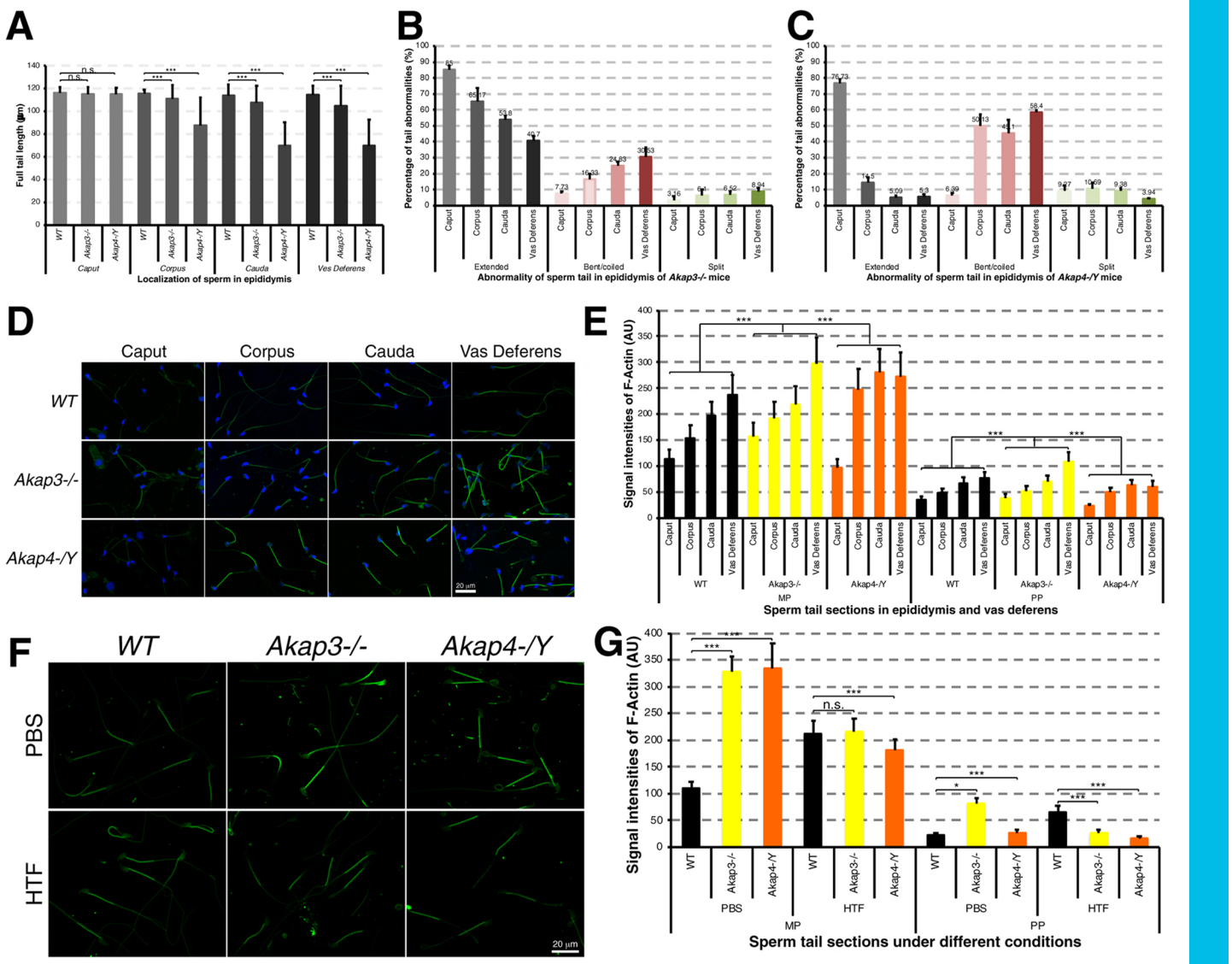

Fig. 7. Increased morphological abnormalities and F-actin in sperm during maturation in the epididymis. (A) Tail length measurement during maturation of sperm in epididymis. The decrease in tail length is more dramatic in *Akap4* null sperm. ***P<0.001 (Student's *t*-test, n=23-300). (B,C) Abnormalities of the sperm tail gained during maturation in the epididymis of *Akap3*$^{-/-}$ and *Akap4*$^{-/Y}$ mice. The increase of tail abnormalities is greater in *Akap4* null sperm, in which the entire FS is missing. Numbers above the bars indicate the average percentages of each abnormality counted within a sperm population (n=4 experimental repeats). (D,E) Elevated F-actin during post-testicular maturation. Sperm from wild-type, *Akap3*$^{-/-}$ and *Akap4*$^{-/Y}$ mice were stained with Phalloidin-FITC. Representative confocal images are shown in D. Quantification of F-actin fluorescent signals in sperm tails are shown in E. ***P<0.001 (Student's *t*-test, n=150-180). The increases in both *Akap3* (yellow) and *Akap4* (orange) null sperm were more dramatic, compared with that of wild-type sperm, as sperm traverse through the epididymis. Sperm nuclei were stained with DAPI. (F,G) Changes of F-actin during capacitation of sperm. Sperm from wild-type, *Akap3*$^{-/-}$ and *Akap4*$^{-/Y}$ mice were stained with Phalloidin-FITC after they were incubated in either PBS or HTF. No further increases of F-actin were seen for mutant sperm after capacitation. *P<0.05, ***P<0.001 (Student's *t*-test, n=160-190). AU, arbitrary units; n.s., not significant; WT, wild type. Representative confocal images are shown in F. Quantification of fluorescent signals of F-actin are shown in G. Scale bars: 20 µm.

during this process until sperm reached the vas deferens (Fig. 7D, top panels, 7E). Interestingly, F-actin signals were not only higher in *Akap3* and *Akap4* mutant sperm in caput epididymis but also increased during the post-testicular maturation process (Fig. 7D, middle and bottom panels, 7E). Fluorescent signals of F-actin were nearly doubled for both wild type and mutants when sperm reached the vas deferens, indicating enhanced formation of F-actin during post-testicular maturation. It has been suggested that F-actin filaments are increased during hyperactivation of sperm (Brener et al., 2003). To evaluate the relationship between F-actin and hyperactivity loss in mutant sperm, sperm treated under different conditions were immunostained with Phalloidin-FITC. Consistent with previous findings, an increase of F-actin could be seen in wild-type sperm when they were incubated in HTF. However, no further increase of F-actin was observed in mutant sperm when they were induced for capacitation, even when they contained higher initial levels of F-actin (Fig. 7F,G). Together, these results suggest that misregulated actin polymerization in mutant sperm accompanies the morphological defects that occur during post-testicular maturation, which may lead to disrupted cellular events that are vital for sperm motility.

DISCUSSION

The primary defects caused by the *Akap3* or *Akap4* mutations are related to sperm morphology; the data presented here suggest that although both AKAPs are important for the formation of a complete FS, they are involved in different pathways affecting different

Development (2020) 147, dev181057. doi:10.1242/dev.181057

subcellular structures. Based on microscopic analyses of developing spermatids, Clermont et al. suggested that components of sperm flagella are synthesized and assembled in sequential order during spermiogenesis (Clermont et al., 1990; Irons and Clermont, 1982). Supporting this hypothesis, the absence of AKAP3 mainly abolished the CRs of FS, whereas AKAP4 is important for the formation of the entire FS (Fig. 3) (Fang et al., 2019; Miki et al., 2002), indicating that subcellular structures of FS could be synthesized independently. Numerous proteins have been identified in the FS, and the functional roles of some of these proteins have been studied through targeted gene deletions in mice (Matzuk and Lamb, 2008). However, the morphological defects elicited by these gene mutations are not exactly the same, reflecting their varied functions during spermiogenesis. Further research is required to find out how they take part in the assembly of various compartments of the flagellum and accomplish the morphological changes of sperm during spermiogenesis.

It remains to be determined what protein components compose different subcellular structures in sperm. The FS is believed to be where signal transduction and glycolytic reactions occur during the regulation of sperm motility. In the same vein, numerous proteins that are known FS components, including PKA signaling factors and motility regulators, were reduced in *Akap3* null sperm, some of which have been shown to interact with AKAP3 directly, such as SPA17, ROPN1 and CABYR (Carr et al., 2001; Li et al., 2011). In addition, proteins that have been suggested to be involved in the final stages of sperm development, such as MFGE8 and SPERT (Feige et al., 2002; Martin-DeLeon, 2006), are enriched in *Akap3* null sperm. Interestingly, proteins that are associated with RNA metabolism and protein synthesis are also enriched in *Akap3* null sperm. This could be caused by either retention of proteins due to the malformation of the FS or increased expression in the absence of AKAP3 during spermiogenesis. Several proteome studies of sperm have shown that mature sperm contain various components of translation machinery, including ribosomal proteins and translation initiation and elongation factors (Chauvin et al., 2012; Skerget et al., 2015). Although some early studies have suggested that nascent proteins could be synthesized within the cytoplasm of spermatids where the future FS is assembled, whether proteins are transported into the flagellum or synthesized locally in the developing sperm tail due to the presence of active translation machinery remains to be determined (Clermont et al., 1990; Oko and Clermont, 1989; San Agustin et al., 2015). The data presented here could provide a hint about how spermatids coordinate protein synthesis with cellular morphogenesis via signaling pathways including PKA.

In mature sperm, the absence of AKAPs disrupted the expression and localization of PKA subunits, both of which contribute to the misregulated PKA activity. Owing to the lack of antibodies that are suitable for immunocytochemical analysis, the subcellular localization of RIα in sperm remains to be determined. However, it is likely that type I PKA is distributed in both soluble and insoluble compartments of the FS and also participates in regulating sperm motility. This notion is supported by the findings that *Akap3* null sperm had decreased PKA activity and phospho-protein levels when mutant sperm were capacitated *in vitro* (Fig. 4). Similarly, *Akap4* null sperm contain mislocalized PKA Cα (Fig. 4G) and increased protein phosphatase activity as shown previously (Huang et al., 2005). It should be noted that in all sperm examined under various conditions, PKA RIIα appeared to be associated with insoluble fractions of mature sperm and localized in the center of flagella. It will be of interest to find out whether PKA RIIα is associated with ODFs or the axoneme, in conjunction with sperm-specific PKA Cα2 during sperm motility regulation (Nolan et al., 2004).

Proteins that were affected by *Akap3* mutation are not only associated with the FS but also widely distributed among various cytoplasmic domains, including the nucleus, acrosome, endoplasmic reticulum/Golgi and plasma membrane, indicating that disruption of the FS had a global effect on the cellular organization of sperm. In support of this, some *Akap3* null sperm were found to contain malformed heads and axonemes. This is similar to numerous gene-targeting studies in mice showing that deteriorated morphology of sperm caused by a single gene mutation often includes multi-faceted phenotypes. How the overall morphogenesis of sperm is coordinated is not clear. Interestingly, SEPTIN4, the component of the septin ring that forms the annulus between the mid-piece and the principal piece of the sperm tail was found to be mislocalized in both *Akap3* and *Akap4* null sperm (Fig. S6), suggesting that the integrity of cytoplasmic segmentation of sperm was compromised. One of the main functional protein groups among the increased proteins in *Akap3* mutant sperm contains actin filament modulators, including Rho GTPases. Several F-actin regulators were also found to be increased in *Akap4* null sperm, such as MFGE8, CTTN and FSCN3 (Fig. S4B). Although relationships between several FS components and actin filaments have been suggested (Fiedler et al., 2013; Fujita et al., 2000), for example during capacitation of sperm (Brener et al., 2003), it is not clear whether the dynamics of actin filaments are involved in the morphogenesis of sperm during spermiogenesis (Gervasi et al., 2018). The increased levels of F-actin in *Akap3* and *Akap4* null sperm suggest that the proper organization of cortical actin filaments could be highly relevant to the overall integrity of the subcellular structures of sperm and the global organization of proteins in sperm.

Following spermiogenesis, when spermatids become fully developed, they travel through epididymis to acquire final matured status. This post-testicular maturation was thought to re-model sperm through biochemical processes (Bedford and Calvin, 1974; Breton et al., 2019) and recently was also found to involve non-coding RNA delivery from somatic cells in the epididymis (Conine et al., 2018; Sharma et al., 2018). The subcortical actin filament likely participates in the modifications sperm receive in the epididymis, including membrane adjustments. In support of this, increased F-actin levels were found in sperm as they passed through the epididymis (Fig. 7). However, *Akap3* and *Akap4* null sperm possessed higher levels of F-actin, potentially rendering them less dynamic compared with the wild type. This was demonstrated by the lack of further F-actin formation induced in the mutants as the sperm underwent capacitation. Furthermore, the dysregulated F-actin formation during post-testicular maturation was accompanied by accumulating morphological defects in the sperm, suggesting that the subcellular structures of the FS may play regulatory roles during the dynamic changes of F-actin and that the proper formation of subcortical F-actin filaments is important for sperm morphology and motility. Supporting this, it has been shown that Sertoli cells provide external cues, including actin-based ectocytoplasmic specialization, to facilitate the morphogenesis of sperm (Tang et al., 2016). It will be of interest to find out whether the dynamics of F-actin formation in sperm would facilitate their cellular morphogenesis in response to external signals. This could also be important for understanding of the etiology of many astheno-teratozoospermia diseases. Together, the presented data indicate that the cellular morphogenesis of sperm is a coordinated process of protein synthesis, localization and assembly, of which AKAP3 and AKAP4 play pivotal yet different roles in the formation of the subcellular structures of functional sperm.

Development (2020) 147, dev181057. doi:10.1242/dev.181057

MATERIALS AND METHODS

Mice

For testis and epididymis tissue extraction, spermatogenic cell purification and sperm isolation, adult C57BL/6 mice were used. Animals were first anesthetized with CO_2 and then sacrificed by cervical dislocation. Testes and epididymis were extracted and photographed or used further for tissue sectioning and cell purification. All animal housing and handling was carried out according to IACUC guidelines and that of the Guangzhou Institutes of Biomedicine and Health, Chinese Academy and Sciences (Permit No. 2009017).

Histology of testes, isolation of spermatogenic cells and flow cytometry

For tissue sectioning, extracted testes were fixed in 4% paraformaldehyde/PBS overnight at 4°C, embedded in paraffin and cut into 8-µm sections with a microtome (Leica RM2255). Extracted epididymides were processed in a similar fashion. Tissue sections were then stained with either Hematoxylin/Eosin or processed for immunocytochemistry. Stained tissue sections were examined with a light microscope (Olympus, ABX51) and images were taken for further analyses.

To isolate spermatogenic cells at various developmental stages, testes from adult mice were first removed from the tunica albuginea and then dissociated into single cells using a digestive enzyme method as described previously (Bellvé, 1993). Briefly, de-capsulated testes were rinsed and then cut into small pieces in pre-warmed DMEM Basic media (Thermo Fisher Scientific). Collagenase IV (Worthington) and DNase I (Worthington) were then added at final concentrations of 2 mg/ml and 5 µg/ml, respectively, and testes were incubated for 15 min in an incubator with 5% CO_2 at 37°C. Cells were dispersed with gentle pipetting every 5 min. Trypsin (Worthington) was then added to the mixture at 0.5 µg/ml and incubation continued for 30 min with occasional pipetting. Dispersed cells were collected by centrifugation at 1000 rpm (178 ***g***) for 10 min at room temperature (RT) with a table centrifuge (Zonkia, SC-3610). Cells were rinsed once and re-suspended with cold PBS. Dispersed cells were then laid on top of a prepared 2-4% bovine serum albumin (BSA) gradient and sedimented for 3 h at RT. Five-milliliter fractions containing spermatocytes, round spermatids or elongating spermatids were collected manually and samples from each fraction were examined under an $Evos_{fl}$ microscope (Advanced Microscopy Group). Similar cell types were pooled together and used for immunocytochemistry.

Flow cytometry of spermatogenic cells was performed as previously described (Bastos et al., 2005). Briefly, dispersed testicular cells were re-suspended in Hanks' Balanced Salt Solution (Gibco, 14025-090), containing 10 µg/ml Hoechst 33342 (Invitrogen, H1311) and 5% fetal bovine serum (Gibco, 10099-141), and incubated in an incubator with 5% CO_2 for 20 min, at 32°C. Propidium iodide (Sigma-Aldrich, P4170) was added at 2 µg/ml. After brief incubation, cells were filtered through a 70-µm cell strainer (Falcon, 08-771-2). Flow cytometry was carried out on a flow cytometer (BD LSRFortessa SORP, BD Biosciences), using Hoechst Blue and Red as parameters. Forward scattering was also implemented in order to separate the round and elongating spermatids.

Generation of *Akap3* and *Akap4* gene knockout mice

Gene knockout in mice was carried out using the CRISPR/Cas9 method. For *Akap3*, two sgRNAs (Table S1) targeting the fifth exon of the *Akap3* genomic coding region were selected using CRISPR Finder from WTSI Genome Editing (WGE) (www.sanger.ac.uk). cDNA fragments encoding the sgRNAs were synthesized and cloned into plasmid pT7-gRNA. cDNA encoding the SpCAS9 endonuclease was from Addgene (Addgene, #51307). The messenger RNA of SpCAS9 was *in vitro* transcribed and purified using the mMESSAGE mMACHINE SP6 kit (Ambion, AM1340) and RNeasy Micro kit (Qiagen, 74004), respectively. sgRNAs were *in vitro* transcribed and purified using the MAXI script T7 kit (Ambion, AM1312) and mirVanaTM miRNA isolation kit (Ambion, AM1561), respectively. Mouse two-cell embryos were isolated from super-ovulated 4- to 6-week-old female mice mated with 2-month-old male mice according to standard procedures. RNA mixture (SpCAS9 mRNA:sgRNA=1:3) were microinjected into the cytoplasm of two-cell embryos. Injected two-cell embryos were then transplanted into the oviduct of pseudo-pregnant foster female CD1 mice. Live animals born after 3 weeks were genotyped for the presence of *Akap3* mutations by PCR and DNA sequencing, using primers flanking the targeted region (F: 5′-ACACATCAACAGATCCTGTC-3′; R: 5′-TGTTCTTGGAACATGCGGTG-3′). Similar experiments were carried out using one sgRNA targeting exon 6 of the *Akap4* gene; genotyping of mutant mice was carried out with primers flanking the targeted region (F: 5′-TGTT-CTATGGACGACCTTTCC-3′; R: 5′-GCTTCCACCTTCCAATTTGTC-3′). Sperm from several male mice carrying insertion/deletion mutations on both alleles were analyzed first after 2-3 months. From various mutants of *Akap3* mice, one female mouse carrying a single allele 103-bp deletion was chosen for further breeding in order to establish the stable gene knockout mouse line. For *Akap4*, a mouse carrying a 16-bp deletion was chosen for further breeding. Off-target effects of sgRNAs were examined by PCR and DNA sequencing for the top putative off-target sites predicted by CRISPR Finder. No mutation was found for the 22 and seven top putative off-target sites of *Akap3* and *Akap4* sgRNAs, respectively (Table S1). Genotypes of either *Akap3* or *Akap4* mutants were determined by PCR of mouse tail genomic DNA using gene-specific primers listed above. The expression of AKAP3 and AKAP4 proteins were further examined in testis and sperm lysates by western blotting and immunofluorescence staining. After the mutant mouse lines were established, 3-month-old male or female mice with different genotypes were mated in various combinations, the litter size and the number of litters generated from three mating pairs of each combination were recorded for a 3-month time period in order to evaluate the effect of gene deletion on fertility.

Light microscopy and transmission electron microscopy (TEM)

To examine the morphology of sperm, sperm from caput, corpus, cauda epididymis and vas deferens were extracted and spread on glass slides. They were mounted in 50% glycerol/PBS and imaged using an inverted light microscope (Olympus, IX71) equipped with a CCD camera. The length of the sperm tail was measured using DP2-BSM software (Olympus). Sperm with extended posture were measured. Sperm with bent/coiled or split flagella were counted within a population of sperm. For TEM, sperm samples from vas deferens or seminiferous tubules were squeezed out and washed in PBS and then fixed in 2.5% glutaraldehyde/PBS overnight at 4°C. They were then washed three times with PBS and fixed again in 1% OsO_4 for 90 min at 4°C. Fixed sperm were dehydrated through a series of decreasing concentrations of ethanol, infiltrated and embedded in Eponate 12 (Tedpella, 18012). Ultra-thin sections were cut at 100 nm using an Ultramicrotome (Leica UC7) and mounted onto copper grids. The grids were then stained in 10% uranyl acetate/methanol for 20 min, and then in lead citrate for 15 min. Stained sections were examined and photographed with a Tecnai G2 Spirit transmission electron microscope (FEI).

Immunocytochemistry, confocal laser-scanning microscopy and STED

Frozen mouse testis sections, isolated sperm and fractionated testicular cells were stained with various antibodies following similar procedures. Briefly, samples were first fixed in cold acetone for 5 min. They were then washed three times with PBST (phosphate-buffered saline containing 0.05% Tween-20, pH 7.4) and blocked in 2% BSA/PBST for 1 h at RT. Primary antibodies were diluted in 1% BSA/PBST and used to incubate blocked samples for 2 h at RT or overnight at 4°C. After washing with PBST three times, 10 min each, samples were incubated with appropriate secondary antibodies in 1% BSA/PBST for 1 h at RT and then washed again three times, 10 min each, with PBST. The samples were then mounted on glass slides in 50% glycerol/PBS. Primary and secondary antibodies used are listed in Table S2. Immunofluorescently stained samples were examined by confocal laser-scanning microscopy (Zeiss, 710 NLO). Intensities of fluorescent signals of either F-actin or phospho-proteins were measured using ZEN-2012SP2-blue software. The same areas of interest were selected for the entire mid-piece and initial segments of the principal piece where sperm tails were usually completely flattened on the surface of glass slides. Average intensities were measured as pixels/unit area. A background area of the same size was also measured in order to subtract non-specific signals. About 150-200 sperm tails for each experiment were analyzed from confocal images. For super-resolution imaging of immunostained sperm, STED was performed on a TCS

Development (2020) 147, dev181057. doi:10.1242/dev.181057

SP8 STED super-resolution microscope system (Leica). Images taken were further processed by de-convolution using Huygens Professional software.

GST pull-down, sperm protein extraction, immunoprecipitation and western blotting

Interactions between AKAP3 and AKAP4 and enolase proteins were examined using a GST pull-down assay. Recombinant AKAP proteins fused with GST tags or enolase with histidine (HIS) tags were expressed in the bacteria *Escherichia coli*. Plasmids encoding GST- or HIS-tagged proteins were first cloned in pGEX-4T-2 and pET-32a vectors, respectively, using gene-specific primers. Positive clones were verified by direct DNA sequencing. After transformation of plasmids into BL21 bacteria, recombinant proteins were induced with 0.1 mM isopropyl β-D-1-thiogalactopyranoside (IPTG) at 16°C overnight. GST fusion proteins were purified from bacterial lysates using glutathione agarose beads (GeneScript, L00206). Purified proteins were examined by SDS-PAGE and Ponceau Red staining (Beyotime, P0022). Bacterial lysates containing HIS-tagged enolase 1 or enolase 4 were mixed with GST fusion proteins for 2 h at 4°C and protein complexes were then pulled down with glutathione agarose beads. GST tag alone was used as the control. Following washing, proteins contained in the pull-down complexes were examined by western blotting after SDS-PAGE. Primers used for constructing plasmids encoding recombinant proteins were: GST-AKAP3 (F: 5′-CGGGATCCATGGCGG-ATAGGGTTGACTGG-3′; R: 5′-ACGCGTCGACCAGGTTTGCCATCA-GCCAG-3′), GST-proAKAP4 (F: 5′-CGGGATCCATGATTGCCTACTGT-GGTACTAC-3′; R: 5′-ACGCGTCGACCAGGTTAGCGAGAAGCCAGT-C-3′), GST-AKAP4 (F: 5′-CGGGATCCATGGCGGCATCCAAAAACAC-CAAC-3′; R: 5′-ACGCGTCGACCAGGTTAGCGAGAAGCCAGTC-3′), HIS-ENO1 (F: 5′-CGGAATTCATGTCTATTCTCAGGATCCACGCCA-3′; R: 5′-CGCAAGCTTTTTGGCCAGGGGGTTCCTGAAG-3′) and HIS-ENO4 (F: 5′-CGGGATCCATGGGAGATGAAGACGGCG-3′; R: 5′-AC-GCGTCGACTGTTTTAGCCGATTCCTCTATCAC-3′). Restriction enzyme digestion sites used for subcloning are underlined.

To extract soluble proteins from testes or sperm, samples were homogenized in cell lysis buffer [20 mM Tris-HCl, pH 8.0, 150 mM NaCl, 2 mM EDTA, 5% glycerol, 1× protease inhibitor cocktail (Roche, 04693132001)], containing 1% Triton X-100 and incubated for 30 min at 4°C. Tissue or cell lysates were centrifuged for 10 min at 13,000 rpm (15,700 ***g***) at 4°C using a tabletop centrifuge (Eppendorf, Centrifuge 5427R). Supernatants containing soluble proteins were transferred into fresh Eppendorf tubes and cell lysis buffer containing 1% SDS was then added to the pellets. Pellets were incubated for 1 h at RT in order to extract insoluble sperm proteins. Protein concentrations of the lysates were measured using a BCA assay kit (Beyotime, P0012S) and stored at −20°C for long-term use.

For the analysis of serine/threonine-phosphorylated proteins of PKA substrates, total sperm protein extraction was carried out using cell lysis buffer containing 1% SDS. For the analysis of tyrosine-phosphorylated proteins, sperm collected with or without capacitation were homogenized in cell lysis buffer, containing 1% Triton X-100 and 1× PhosSTOP protein phosphatase inhibitor cocktail (Roche, 04906837001) and incubated for 30 min at 4°C, with occasional vortexing. The sperm lysates were then centrifuged for 12 min at 13,000 rpm (15,700 ***g***) at 4°C. After removing the supernatant, pellets were re-suspended in protein sample buffer (2% SDS) and incubated for 1 h at RT, then boiled for 10 min to completely dissolve insoluble sperm proteins before SDS-PAGE and western blotting. To examine tyrosine-phosphorylated AKAP3, sperm and testes were lysed in cell lysis buffer containing 0.1% SDS, 5 mM DTT and 1× PhosSTOP protein phosphatase inhibitor cocktail, at RT for 2 h, with sonication (ten rounds of 1 s run, 5 s interval) every 20 min. Cell lysates were then diluted at 1:50 with cell lysis buffer containing 1% Triton X-100 and incubated with anti-AKAP3 at 1:25 overnight at 4°C. Immunoprecipitates were then brought down using Protein G-agarose beads (GenScript, L00209) and subjected to western blotting. Western blotting was carried out for all protein samples by separating by SDS-PAGE, transferring onto nitrocellulose membranes and incubating membranes with various antibodies accordingly (Table S2). Following incubation with horseradish peroxidase (HRP)-conjugated secondary antibodies, signals were detected using SuperSignalTM West Pico PLUS (Thermo Scientific, 34577) (Xu and Qi, 2014).

PKA activity assay

PKA kinase activity in sperm was measured according to the manufacturer's instructions (Arbor Assays, K027-H1). About 1×10^7 sperm were homogenized in 1 ml cell lysis buffer, containing 1% NP40 and 1× PhosSTOP protein phosphatase inhibitor cocktail for 30 min on ice with occasional vortexing. Sperm lysates were centrifuged at 10,000 rpm (9300 ***g***) at 4°C for 10 min and supernatants were transferred into fresh tubes. Protein concentration was measured using a BCA assay kit. Supernatants were then diluted to 1 µg/ml protein concentration with kinase buffer and 40 µl of each sample was transferred into one well of a 96-well plate. Ten microliters of re-suspended ATP was added to each well and the plate was sealed and shaken for 90 min at 30°C. Reacted solutions were then aspirated out and the plate was washed with the wash buffer included in the PKA Assay kit (300 µl/per well) four times. The plate was tapped dry on clean absorbent towel and 25 µl of rabbit phospho-PKA substrate antibody and 25 µl of goat-anti-rabbit IgG HRP conjugate from the kit were then added to each well. The plate was sealed and shaken for 60 min at RT and washed again as above. TMB Substrate Solution (100 µl) was added to each well and incubated for 30 min at RT. Stop Solution (50 µl) was then added to each well and the plate was read at 450 nm using a luminescent spectrometer (Monochromator Multimode Microplate Reader, Berthold, Mithras LB 943). Recombinant PKA Cα supplied by the manufacturer was used in parallel in order to draw a standard curve of PKA activity.

Capacitation of sperm *in vitro* and comparison of sperm motility

Sperm from adult mice were collected from the vas deferens by squeezing them out in PBS. Sperm were pelleted by centrifugation at 500 rpm (44 ***g***) for 5 min at RT, washed once with PBS and re-suspended in PBS at a concentration of 2×10^6 cells/ml. To induce capacitation in sperm, roughly 2×10^6 sperm cells were re-suspended in 1 ml HTF (Millipore, MR-070-D) and transferred into each well of a 24-well plate and incubated in a 37°C incubator with 5% CO_2 for 2 h. After the incubation, the motility of sperm from wild-type, *Akap3* or *Akap4* mutant mice were examined under basal (PBS) and capacitation (HTF) conditions and recorded using an inverted light microscope (Olympus, IX71) equipped with a CCD camera (Movies 1-6).

Tandem mass spectrometry of the sperm proteome

Quantitative proteomics of sperm proteins was performed according to standard procedures of Tandem Mass Tag and LC-MS/MS. Briefly, sperm from the vas deferens of adult mice (2-3 months old) were collected and washed in hypotonic solution (Red Blood Cell Lysis Buffer, Beyotime, C3702) in order to get rid of contaminating blood cells. Total protein was extracted from sperm under denaturing conditions (8 M urea, 1% Protease Inhibitor Cocktail). Protein concentrations of cell lysates were measured using the BCA method and an equal amount of protein from the sperm of wild-type, *Akap3*$^{-/-}$ or *Akap4*$^{-/Y}$ mice were taken and digested with trypsin. Tryptic peptides were labeled using the TMT kit/iTRAQ kit and a mixture of labeled peptides were fractionated by high pH reverse-phase HPLC into 18 fractions and subjected to LC-MS/MS identification. Three experimental repeats were carried out for the mass spectrometry using wild-type, *Akap3*$^{-/-}$ and *Akap4*$^{-/Y}$ mice (six of each genotype, total of 18 mice) at either the same time or at different times. Raw mass spectrometry data were processed using the Maxquant search engine and proteins were matched to the SwissProt Mouse Database. Quantification of differentially expressed proteins was analyzed further using standard procedures according to the peptides identified by MS/MS. Proteins identified in two experimental repeats and that showed changes ≥1.3-fold (P>0.05) were further analyzed by bioinformatics (Tables S3, S4). Protein extraction, peptide preparation and LC-MS/MS were performed by PTM Biolabs (Hangzhou, China).

Bioinformatics and statistical analysis

GO annotations were obtained using online DAVID Bioinformatics Resources 6.8 (https://david.ncifcrf.gov). The heat map was generated with protein fold changes using the online source Morpheus at http://software.broadinstitute.org/morpheus. The over-represented Reactome pathways were analyzed using Panther (www.pantherdb.org) and protein-protein interaction networks were further processed using String (www.string-db.org). Annotations of protein-protein interaction networks and proteins that are related to over-

represented functional units were analyzed and presented using Cytoscape 3.7.1 and integrated script ClueGo (Bindea et al., 2009). Statistical analyses of sperm tail lengths, abnormalities of sperm tail, F-actin levels, phosphoprotein levels and PKA activities were performed using two-tailed Student's *t*-test; significances were set as ***P<0.001, **P<0.01 and *P<0.05. Data are presented as mean+s.d. and plotted using Excel software.

Acknowledgements
We would like to thank Jinyue Liao and Tin-Lap Lee for their advice on bioinformatics analyses. We also thank our lab members for their discussions and support through the course of this work.

Competing interests
The authors declare no competing or financial interests.

Author contributions
Conceptualization: K.X., L.Y., H.Q.; Methodology: K.X., L.Y., H.Q.; Validation: K.X., L.Y., H.Q.; Formal analysis: K.X., L.Y., H.Q.; Investigation: K.X., L.Y., H.Q.; Resources: L.Z., H.Q.; Data curation: K.X., L.Y., L.Z., H.Q.; Writing - original draft: K.X., H.Q.; Writing - review & editing: L.Z., H.Q.; Visualization: H.Q.; Supervision: H.Q.; Project administration: H.Q.; Funding acquisition: L.Z., H.Q.

Funding
This work is supported by the National Key Research and Development Program of China from the Ministry of Science and Technology of the People's Republic of China (2018YFC1004700), the Frontier Research Program of Guangzhou Regenerative Medicine and Health Guangdong Laboratory (2018GZR110105021), the Guangdong Provincial Key Laboratory of Stem Cell and Regenerative Medicine (2017B030314056) and Guangzhou Medical University (B195002005009), and is partly supported by the Chinese Academy of Sciences.

Data availability
The mass spectrometry proteomics data have been deposited to the ProteomeXchange Consortium via the PRIDE [1] partner repository with the dataset identifier PXD016928 (Perez-Riverol et al., 2019).

Supplementary information
Supplementary information available online at
http://dev.biologists.org/lookup/doi/10.1242/dev.181057.supplemental

References
Baccetti, B., Collodel, G., Estenoz, M., Manca, D., Moretti, E. and Piomboni, P. (2005). Gene deletions in an infertile man with sperm fibrous sheath dysplasia. *Hum. Reprod.* **20**, 2790-2794. doi:10.1093/humrep/dei126

Baker, M. A., Hetherington, L., Curry, B. and Aitken, R. J. (2009). Phosphorylation and consequent stimulation of the tyrosine kinase c-Abl by PKA in mouse spermatozoa; its implications during capacitation. *Dev. Biol.* **333**, 57-66. doi:10.1016/j.ydbio.2009.06.022

Bastos, H., Lassalle, B., Chicheportiche, A., Riou, L., Testart, J., Allemand, I. and Fouchet, P. (2005). Flow cytometric characterization of viable meiotic and postmeiotic cells by Hoechst 33342 in mouse spermatogenesis. *Cytometry A* **65A**, 40-49. doi:10.1002/cyto.a.20129

Bedford, J. M. and Calvin, H. I. (1974). Changes in -S-S- linked structures of the sperm tail during epididymal maturation, with comparative observations in sub-mammalian species. *J. Exp. Zool.* **187**, 181-204. doi:10.1002/jez.1401870202

Bellvé, A. R. (1993). Purification, culture, and fractionation of spermatogenic cells. *Methods Enzymol.* **225**, 84-113. doi:10.1016/0076-6879(93)25009-Q

Bindea, G., Mlecnik, B., Hackl, H., Charoentong, P., Tosolini, M., Kirilovsky, A., Fridman, W. H., Pages, F., Trajanoski, Z. and Galon, J. (2009). ClueGO: a Cytoscape plug-in to decipher functionally grouped gene ontology and pathway annotation networks. *Bioinformatics* **25**, 1091-1093. doi:10.1093/bioinformatics/btp101

Bragg, P. W. and Handel, M. A. (1979). Protein synthesis in mouse spermatozoa. *Biol. Reprod.* **20**, 333-337. doi:10.1095/biolreprod20.2.333

Braun, R. E., Peschon, J. J., Behringer, R. R., Brinster, R. L. and Palmiter, R. D. (1989). Protamine 3'-untranslated sequences regulate temporal translational control and subcellular localization of growth hormone in spermatids of transgenic mice. *Genes Dev.* **3**, 793-802. doi:10.1101/gad.3.6.793

Brener, E., Rubinstein, S., Cohen, G., Shternall, K., Rivlin, J. and Breitbart, H. (2003). Remodeling of the actin cytoskeleton during mammalian sperm capacitation and acrosome reaction. *Biol. Reprod.* **68**, 837-845. doi:10.1095/biolreprod.102.009233

Burton, K. A., McDermott, D. A., Wilkes, D., Poulsen, M. N., Nolan, M. A., Goldstein, M., Basson, C. T. and McKnight, G. S. (2006). Haploinsufficiency at the protein kinase A RIα gene locus leads to fertility defects in male mice and men. *Mol. Endocrinol.* **20**, 2504-2513. doi:10.1210/me.2006-0060

Breton, S., Nair, A. V. and Battistone, M. A. (2019). Epithelial dynamics in the epididymis: role in the maturation, protection, and storage of spermatozoa. *Andrology* **7**, 631-643. doi:10.1111/andr.12632

Burton, K. A. and McKnight, G. S. (2007). PKA, germ cells, and fertility. *Physiology (Bethesda)* **22**, 40-46. doi:10.1152/physiol.00034.2006

Carr, D. W., Fujita, A., Stentz, C. L., Liberty, G. A., Olson, G. E. and Narumiya, S. (2001). Identification of sperm-specific proteins that interact with A-kinase anchoring proteins in a manner similar to the type II regulatory subunit of PKA. *J. Biol. Chem.* **276**, 17332-17338. doi:10.1074/jbc.M011252200

Carrera, A., Gerton, G. L. and Moss, S. B. (1994). The major fibrous sheath polypeptide of mouse sperm: structural and functional similarities to the A-kinase anchoring proteins. *Dev. Biol.* **165**, 272-284. doi:10.1006/dbio.1994.1252

Castaneda, J. M., Hua, R., Miyata, H., Oji, A., Guo, Y., Cheng, Y., Zhou, T., Guo, X., Cui, Y., Shen, B. et al. (2017). TCTE1 is a conserved component of the dynein regulatory complex and is required for motility and metabolism in mouse spermatozoa. *Proc. Natl. Acad. Sci. USA* **114**, E5370-E5378. doi:10.1073/pnas.1621279114

Chauvin, T., Xie, F., Liu, T., Nicora, C. D., Yang, F., Camp, D. G., II, Smith, R. D. and Roberts, K. P. (2012). A systematic analysis of a deep mouse epididymal sperm proteome. *Biol. Reprod.* **87**, 1-8. doi:10.1093/biolreprod/87.s1.1

Clermont, Y., Oko, R. and Hermo, L. (1990). Immunocytochemical localization of proteins utilized in the formation of outer dense fibers and fibrous sheath in rat spermatids: an electron microscope study. *Anat. Rec.* **227**, 447-457. doi:10.1002/ar.1092270408

Conine, C. C., Sun, F., Song, L., Rivera-Pérez, J. A. and Rando, O. J. (2018). Small RNAs gained during epididymal transit of sperm are essential for embryonic development in mice. *Dev. Cell* **46**, 470-480.e473. doi:10.1016/j.devcel.2018.06.024

Coutton, C., Escoffier, J., Martinez, G., Arnoult, C. and Ray, P. F. (2015). Teratozoospermia: spotlight on the main genetic actors in the human. *Hum. Reprod. Update* **21**, 455-485. doi:10.1093/humupd/dmv020

Eddy, E. M., Toshimori, K. and O'Brien, D. A. (2003). Fibrous sheath of mammalian spermatozoa. *Microsc. Res. Tech.* **61**, 103-115. doi:10.1002/jemt.10320

Fang, X., Huang, L.-L., Xu, J., Ma, C.-Q., Chen, Z.-H., Zhang, Z., Liao, C.-H., Zheng, S.-X., Huang, P., Xu, W.-M. et al. (2019). Proteomics and single-cell RNA analysis of Akap4-knockout mice model confirm indispensable role of Akap4 in spermatogenesis. *Dev. Biol.* **454**, 118-127. doi:10.1016/j.ydbio.2019.06.017

Feige, E., Chen, A. and Motro, B. (2002). Nurit, a novel leucine-zipper protein, expressed uniquely in the spermatid flower-like structure. *Mech. Dev.* **117**, 369-377. doi:10.1016/S0925-4773(02)00217-4

Fiedler, S. E., Dudiki, T., Vijayaraghavan, S. and Carr, D. W. (2013). Loss of R2D2 proteins ROPN1 and ROPN1L causes defects in murine sperm motility, phosphorylation, and fibrous sheath integrity. *Biol. Reprod.* **88**, 41. doi:10.1095/biolreprod.112.105262

Fujita, A., Nakamura, K., Kato, T., Watanabe, N., Ishizaki, T., Kimura, K., Mizoguchi, A. and Narumiya, S. (2000). Ropporin, a sperm-specific binding protein of rhophilin, that is localized in the fibrous sheath of sperm flagella. *J. Cell Sci.* **113**, 103-112.

Fulcher, K. D., Mori, C., Welch, J. E., O'Brien, D. A., Klapper, D. G. and Eddy, E. M. (1995). Characterization of Fsc1 cDNA for a mouse sperm fibrous sheath component. *Biol. Reprod.* **52**, 41-49. doi:10.1095/biolreprod52.1.41

Gervasi, M. G., Xu, X., Carbajal-Gonzalez, B., Buffone, M. G., Visconti, P. E. and Krapf, D. (2018). The actin cytoskeleton of the mouse sperm flagellum is organized in a helical structure. *J. Cell Sci.* **131**, jcs215897. doi:10.1242/jcs.215897

Gitlits, V. M., Toh, B. H., Loveland, K. L. and Sentry, J. W. (2000). The glycolytic enzyme enolase is present in sperm tail and displays nucleotide-dependent association with microtubules. *Eur. J. Cell Biol.* **79**, 104-111. doi:10.1078/S0171-9335(04)70012-6

Gold, H. B., Jung, Y. H. and Corces, V. G. (2018). Not just heads and tails: the complexity of the sperm epigenome. *J. Biol. Chem.* **293**, 13815-13820. doi:10.1074/jbc.R117.001561

Hermo, L., Pelletier, R.-M., Cyr, D. G. and Smith, C. E. (2010). Surfing the wave, cycle, life history, and genes/proteins expressed by testicular germ cells. Part 3: developmental changes in spermatid flagellum and cytoplasmic droplet and interaction of sperm with the zona pellucida and egg plasma membrane. *Microsc. Res. Tech.* **73**, 320-363. doi:10.1002/jemt.20784

Huang, Z., Somanath, P. R., Chakrabarti, R., Eddy, E. M. and Vijayaraghavan, S. (2005). Changes in intracellular distribution and activity of protein phosphatase PP1gamma2 and its regulating proteins in spermatozoa lacking AKAP4. *Biol. Reprod.* **72**, 384-392. doi:10.1095/biolreprod.104.034140

Iguchi, N., Tobias, J. W. and Hecht, N. B. (2006). Expression profiling reveals meiotic male germ cell mRNAs that are translationally up- and down-regulated. *Proc. Natl. Acad. Sci. USA* **103**, 7712-7717. doi:10.1073/pnas.0510999103

Irons, M. J. and Clermont, Y. (1982). Kinetics of fibrous sheath formation in the rat spermatid. *Am. J. Anat.* **165**, 121-130. doi:10.1002/aja.1001650204

Johnson, L. R., Foster, J. A., Haig-Ladewig, L., VanScoy, H., Rubin, C. S., Moss, S. B. and Gerton, G. L. (1997). Assembly of AKAP82, a protein kinase A anchor protein, into the fibrous sheath of mouse sperm. *Dev. Biol.* **192**, 340-350. doi:10.1006/dbio.1997.8767

Kleene, K. C. (2013). Connecting cis-elements and trans-factors with mechanisms of developmental regulation of mRNA translation in meiotic and haploid mammalian spermatogenic cells. *Reproduction* **146**, R1-R19. doi:10.1530/REP-12-0362
Krausz, C. and Riera-Escamilla, A. (2018). Genetics of male infertility. *Nat. Rev. Urol.* **15**, 369-384. doi:10.1038/s41585-018-0003-3
Leblond, C. P. and Clermont, Y. (1952). Spermiogenesis of rat, mouse, hamster and guinea pig as revealed by the periodic acid-fuchsin sulfurous acid technique. *Am. J. Anat.* **90**, 167-215. doi:10.1002/aja.1000900202
Lehti, M. S. and Sironen, A. (2017). Formation and function of sperm tail structures in association with sperm motility defects. *Biol. Reprod.* **97**, 522-536. doi:10.1093/biolre/iox096
Li, Y. F., He, W., Mandal, A., Kim, Y. H., Digilio, L., Klotz, K., Flickinger, C. J., Herr, J. C. and Herr, J. C. (2011). CABYR binds to AKAP3 and Ropporin in the human sperm fibrous sheath. *Asian J. Androl.* **13**, 266-274. doi:10.1038/aja.2010.149
Lin, R.-Y., Moss, S. B. and Rubin, C. S. (1995). Characterization of S-AKAP84, a novel developmentally regulated A kinase anchor protein of male germ cells. *J. Biol. Chem.* **270**, 27804-27811. doi:10.1074/jbc.270.46.27804
Mandal, A., Naaby-Hansen, S., Wolkowicz, M. J., Klotz, K., Shetty, J., Retief, J. D., Coonrod, S. A., Kinter, M., Sherman, N., Cesar, F. et al. (1999). FSP95, a testis-specific 95-kilodalton fibrous sheath antigen that undergoes tyrosine phosphorylation in capacitated human spermatozoa. *Biol. Reprod.* **61**, 1184-1197. doi:10.1095/biolreprod61.5.1184
Martin-DeLeon, P. A. (2006). Epididymal SPAM1 and its impact on sperm function. *Mol. Cell. Endocrinol.* **250**, 114-121. doi:10.1016/j.mce.2005.12.033
Matzuk, M. M. and Lamb, D. J. (2008). The biology of infertility: research advances and clinical challenges. *Nat. Med.* **14**, 1197-1213. doi:10.1038/nm.f.1895
Miki, K., Willis, W. D., Brown, P. R., Goulding, E. H., Fulcher, K. D. and Eddy, E. M. (2002). Targeted disruption of the Akap4 gene causes defects in sperm flagellum and motility. *Dev. Biol.* **248**, 331-342. doi:10.1006/dbio.2002.0728
Nakada, K., Sato, A., Yoshida, K., Morita, T., Tanaka, H., Inoue, S., Yonekawa, H. and Hayashi, J. (2006). Mitochondria-related male infertility. *Proc. Natl. Acad. Sci. USA* **103**, 15148-15153. doi:10.1073/pnas.0604641103
Nakamura, N., Dai, Q., Williams, J., Goulding, E. H., Willis, W. D., Brown, P. R. and Eddy, E. M. (2013). Disruption of a spermatogenic cell-specific mouse enolase 4 (eno4) gene causes sperm structural defects and male infertility. *Biol. Reprod.* **88**, 90. doi:10.1095/biolreprod.112.107128
Nolan, M. A., Babcock, D. F., Wennemuth, G., Brown, W., Burton, K. A. and McKnight, G. S. (2004). Sperm-specific protein kinase A catalytic subunit Calpha2 orchestrates cAMP signaling for male fertility. *Proc. Natl. Acad. Sci. USA* **101**, 13483-13488. doi:10.1073/pnas.0405580101
Oakberg, E. F. (1956). A description of spermiogenesis in the mouse and its use in analysis of the cycle of the seminiferous epithelium and germ cell renewal. *Am. J. Anat.* **99**, 391-413. doi:10.1002/aja.1000990303
Odet, F., Gabel, S. A., Williams, J., London, R. E., Goldberg, E. and Eddy, E. M. (2011). Lactate dehydrogenase C and energy metabolism in mouse sperm. *Biol. Reprod.* **85**, 556-564. doi:10.1095/biolreprod.111.091546
Oko, R. and Clermont, Y. (1989). Light microscopic immunocytochemical study of fibrous sheath and outer dense fiber formation in the rat spermatid. *Anat. Rec.* **225**, 46-55. doi:10.1002/ar.1092250108
Ostermeier, G. C., Dix, D. J., Miller, D., Khatri, P. and Krawetz, S. A. (2002). Spermatozoal RNA profiles of normal fertile men. *Lancet* **360**, 772-777. doi:10.1016/S0140-6736(02)09899-9
Owa, M., Uchihashi, T., Yanagisawa, H. A., Yamano, T., Iguchi, H., Fukuzawa, H., Wakabayashi, K. I., Ando, T. and Kikkawa, M. (2019). Inner lumen proteins stabilize doublet microtubules in cilia and flagella. *Nat. Commun.* **10**, 1143. doi:10.1038/s41467-019-09051-x
Perez-Riverol, Y., Csordas, A., Bai, J., Bernal-Llinares, M., Hewapathirana, S., Kundu, D. J., Inuganti, A., Griss, J., Mayer, G., Eisenacher, M. et al. (2019). The PRIDE database and related tools and resources in 2019: improving support for quantification data. *Nucleic Acids Res.* **47**, D442-D450. doi:10.1093/nar/gky1106
Rawe, V. Y., Ramalho-Santos, J., Payne, C., Chemes, H. E. and Schatten, G. (2004). WAVE1, an A-kinase anchoring protein, during mammalian spermatogenesis. *Hum. Reprod.* **19**, 2594-2604. doi:10.1093/humrep/deh513
San Agustin, J. T., Pazour, G. J. and Witman, G. B. (2015). Intraflagellar transport is essential for mammalian spermiogenesis but is absent in mature sperm. *Mol. Biol. Cell* **26**, 4358-4372. doi:10.1091/mbc.E15-08-0578
Saraswat, M., Joenvaara, S., Jain, T., Tomar, A. K., Sinha, A., Singh, S., Yadav, S. and Renkonen, R. (2017). Human spermatozoa quantitative proteomic signature classifies normo- and asthenozoospermia. *Mol. Cell. Proteomics* **16**, 57-72. doi:10.1074/mcp.M116.061028
Sassone-Corsi, P. (2002). Unique chromatin remodeling and transcriptional regulation in spermatogenesis. *Science* **296**, 2176-2178. doi:10.1126/science.1070963
Scott, J. D., Dessauer, C. W. and Tasken, K. (2013). Creating order from chaos: cellular regulation by kinase anchoring. *Annu. Rev. Pharmacol. Toxicol.* **53**, 187-210. doi:10.1146/annurev-pharmtox-011112-140204
Sharma, U., Sun, F., Conine, C. C., Reichholf, B., Kukreja, S., Herzog, V. A., Ameres, S. L. and Rando, O. J. (2018). Small RNAs are trafficked from the epididymis to developing mammalian sperm. *Dev. Cell* **46**, 481-494.e6. doi:10.1016/j.devcel.2018.06.023
Skerget, S., Rosenow, M. A., Petritis, K. and Karr, T. L. (2015). Sperm proteome maturation in the mouse epididymis. *PLoS ONE* **10**, e0140650. doi:10.1371/journal.pone.0140650
Tang, E. I., Lee, W. M. and Cheng, C. Y. (2016). Coordination of actin- and microtubule-based cytoskeletons supports transport of spermatids and residual bodies/phagosomes during spermatogenesis in the rat testis. *Endocrinology* **157**, 1644-1659. doi:10.1210/en.2015-1962
Torres-Quesada, O., Mayrhofer, J. E. and Stefan, E. (2017). The many faces of compartmentalized PKA signalosomes. *Cell. Signal.* **37**, 1-11. doi:10.1016/j.cellsig.2017.05.012
Vijayaraghavan, S., Liberty, G. A., Mohan, J., Winfrey, V. P., Olson, G. E. and Carr, D. W. (1999). Isolation and molecular characterization of AKAP110, a novel, sperm-specific protein kinase A-anchoring protein. *Mol. Endocrinol.* **13**, 705-717. doi:10.1210/mend.13.5.0278
Visconti, P. E., Johnson, L. R., Oyaski, M., Fornés, M., Moss, S. B., Gerton, G. L. and Kopf, G. S. (1997). Regulation, localization, and anchoring of protein kinase A subunits during mouse sperm capacitation. *Dev. Biol.* **192**, 351-363. doi:10.1006/dbio.1997.8768
Wachten, D., Jikeli, J. F. and Kaupp, U. B. (2017). Sperm sensory signaling. *Cold Spring Harb. Perspect Biol.* **9**, a028225. doi:10.1101/cshperspect.a028225
Xu, K. and Qi, H. (2014). Sperm-specific AKAP3 is a dual-specificity anchoring protein that interacts with both protein kinase a regulatory subunits via conserved N-terminal amphipathic peptides. *Mol. Reprod. Dev.* **81**, 595-607. doi:10.1002/mrd.22329
Xu, K., Yang, L., Zhao, D., Wu, Y. and Qi, H. (2014). AKAP3 synthesis is mediated by RNA binding proteins and PKA signaling during mouse spermiogenesis. *Biol. Reprod.* **90**, 1-14. doi:10.1095/biolreprod.113.116111